



1 Representation of phosphorus cycle in Joint UK Land 2 Environment Simulator (vn5.5_JULES-CNP)

3
4 Mahdi (André) Nakhavali¹, Lina M. Mercado^{1,2}, Iain P. Hartley¹, Stephen Sitch¹, Fernanda V
5 Cunha³, Raffaello di Ponzio³, Laynara F. Lugli³, Carlos A. Quesada³, Kelly M. Andersen^{1,4,5},
6 Sarah E. Chadburn⁶, Andy J. Wiltshire^{1,7}, Douglas B. Clark², Gyovanni Ribeiro³, Lara
7 Siebert³, Anna C. M. Moraes³, Jéssica Schmeisk Rosa³, Rafael Assis³ and José L. Camargo³
8

9 ¹University of Exeter, College of Life and Environmental Sciences, Exeter, EX4 4QE, United Kingdom
10 ²UK Centre for Ecology and Hydrology, Wallingford, OX10 8BB, United Kingdom
11 ³Coordination of Environmental Dynamics, National Institute of Amazonian Research, Manaus, AM 69060-062,
12 Brazil
13 ⁴University of Edinburgh, School of Geosciences, Edinburgh, EH8 9AB, UK
14 ⁵Nanyang Technological University, Asian School of the Environment, Singapore, 639798, Singapore
15 ⁶College of Engineering, Mathematics, and Physical Sciences, University of Exeter, Exeter, EX4
16 4QE, United Kingdom
17 ⁷Met Office Hadley Centre, Exeter, Devon, EX1 3PB, United Kingdom

18 *Correspondence to:* Mahdi (André) Nakhavali (m.nakhavali@exeter.ac.uk)

19 20 Abstract

21
22 Most Land Surface Models (LSMs), the land components of Earth system models (ESMs), include
23 representation of N limitation on ecosystem productivity. However only few of these models have incorporated
24 phosphorus (P) cycling. In tropical ecosystems, this is likely to be particularly important as N tends to be
25 abundant but the availability of rock-derived elements, such as P, can be very low. Thus, without a
26 representation of P cycling, tropical forest response in areas such as Amazonia to rising atmospheric CO₂
27 conditions remains highly uncertain. In this study, we introduced P dynamics and its interactions with the N and
28 carbon (C) cycles into the Joint UK Land Environment Simulator (JULES). The new model (JULES-CNP)
29 includes the representation of P stocks in vegetation and soil pools, as well as key processes controlling fluxes
30 between these pools. We evaluate JULES-CNP at the Amazon nutrient fertilization experiment (AFEX), a low
31 fertility site, representative of about 60% of Amazon soils. We apply the model under ambient CO₂ and elevated
32 CO₂. The model is able to reproduce the observed plant and soil P pools and fluxes under ambient CO₂. We
33 estimate P to limit net primary productivity (NPP) by 24% under current CO₂ and by 46% under elevated CO₂.
34 Under elevated CO₂, biomass in simulations accounting for CNP increase by 10% relative to at contemporary
35 CO₂, although it is 5% lower compared with CN and C-only simulations. Our results highlight the potential for
36 high P limitation and therefore lower CO₂ fertilization capacity in the Amazon forest with low fertility soils.
37



38 **1. Introduction**

39
40 Land ecosystems currently take up about 30% of anthropogenic CO₂ emissions (Friedlingstein *et al.*, 2020), thus
41 buffering the anthropogenic increase in atmospheric CO₂. Tropical forests play a major role in the land carbon
42 (C) cycle, account for about half of global Net Primary Production (NPP)(Schimel *et al.*, 2015), and store the
43 highest above ground carbon among all biomes (Pan *et al.*, 2011; Mitchard, 2018).

44
45 The C sink capacity of tropical forests may be constrained by nutrient availability for plant photosynthesis and
46 growth (Vitousek and Howarth, 1991; Elser *et al.*, 2007; LeBauer and Treseder, 2008) via either P (Nordin,
47 Högberg and Näsholm, 2001; Shen *et al.*, 2011) and/or N related processes (DeLuca, Keeney and McCarty,
48 1992; Perakis and Hedin, 2002). Global process-based models of vegetation dynamics and function suggest a
49 continued land C sink in the tropical forests, largely attributed to the CO₂ fertilization effect (Sitch *et al.*, 2008;
50 Schimel, Stephens and Fisher, 2015; Koch, Hubau and Lewis, 2021). However, many of these models typically
51 do not consider P constraints on plant growth (Fleischer *et al.*, 2019), which is likely to be an important limiting
52 nutrient in tropical ecosystems, characterised by old and heavily weathered soils. The importance of nutrient
53 cycling representation in Earth System Models (ESMs), and the lack thereof, was highlighted by Hungate *et al.*
54 (2003) and Zaehle and Dalmonech (2011), showing the significance of nutrient inclusion in ESMs for
55 generating more realistic estimations of the future evolution of the terrestrial C sink. However, in the Coupled
56 Climate C Cycle Model Inter-comparison Project (C4MIP), none of the participating ESMs included N
57 dynamics (Friedlingstein *et al.*, 2006). Seven years later, for the update in CMIP5 (Anav *et al.*, 2013), three
58 models out of eighteen with N dynamics were included. Although much progress has been made in the inclusion
59 of an N cycle in ESMs so far, none of the CMIP5 models included P cycling and in the most recent CMIP6,
60 only one model includes P (ACCESSES1.5 model) (Arora *et al.*, 2020).

61
62 The long history of soil development in tropical regions which involves the loss of rock-derived nutrients
63 through weathering and leaching on geologic timescales (Vitousek *et al.*, 1997, 2010) results in highly
64 weathered soils. Soil P is hypothesised to be among the key limiting nutrients to plant growth in tropical forests,
65 unlike temperate forest where N is hypothesised to be the main constraint. Low P availability in tropical soils is
66 related to the limited un-weathered parent material or organic compounds as source of P (Walker and Syers,
67 1976), active sorption (Sanchez, 1977) and high occlusion (Yang and Post, 2011) which further reduce plant
68 available P. While N can impact the terrestrial C sink response to increasing atmospheric CO₂ by changing plant
69 C fixation capacity (Luo *et al.*, 2004) via the continuous inputs of N into ecosystems from atmospheric
70 deposition and biological N fixation (Vitousek *et al.*, 2010), the lack of large P inputs into ecosystems and slow
71 rates of P input and output to and from ecosystems, especially those growing on highly weathered soil, makes P
72 limitation a stronger constraint on ecosystems response to elevated CO₂ (eCO₂) than N (Gentile *et al.*, 2012;
73 Sardans, Rivas-Ubach and Peñuelas, 2012). Hence, a separate knowledge is needed to understand how nutrient
74 availability controls tropical compared to the temperate forest productivity. This causes considerable uncertainty
75 in predicting the future of the Amazon forest C sink (Yang *et al.*, 2014).

76
77 There is evidence to suggest P limitation on plant productivity in the Amazon forest (Malhi, 2012) where it has
78 been shown that the younger, more fertile west and south-west Amazon soils have higher tree turnover (Phillips
79 *et al.*, 2004; Stephenson and Van Mantgem, 2005) and stem growth rates (Malhi *et al.*, 2004) and lower above
80 ground biomass (Baker *et al.*, 2004; Malhi *et al.*, 2006) compared to their central and eastern counterparts. Total
81 soil P has been found as the best predictor of stem growth (Quesada *et al.*, 2010) and of total NPP (Aragão *et*
82 *al.*, 2009) across this fertility gradient, and foliar P is positively related to plant photosynthetic capacity (V_{cmax}
83 and J_{cmax}) in these forests (Mercado *et al.*, 2011).

84
85
86 However, modelling studies are unable to reproduce observed spatial patterns of NPP and biomass in the
87 Amazon due to missing processes such as flexible C allocation, spatial variation of biomass turnover (Cleveland
88 *et al.*, 2015) and due to the lack of inclusion of soil P constraints on plant productivity and function. Recent
89 modelling work has focused on improving process and parameter representation using the observational data of
90 spatial variation in woody biomass residence time (Johnson *et al.*, 2016), soil texture and soil P to parameterise
91 the maximum RuBiCo carboxylation capacity (V_{cmax}) (Castanho *et al.*, 2013). Results from these studies
92 successfully represent observed patterns of Amazon forest biomass growth increases with increasing soil
93 fertility. However, the full representation of these interactions and the impact of the soil nutrient availability on
94 biomass productivity is still missing in most of ESMs.



98 So far, several dynamic global vegetation models have been developed to represent P cycling within the soil
99 (Yang *et al.*, 2013; Hou *et al.*, 2019) and between plant and soils for tropical forests particularly (Yang *et al.*,
100 2014; Zhu *et al.*, 2016; Goll *et al.*, 2017). Furthermore, a comprehensive study included several models with C-
101 N-P cycling and their feedbacks on the atmospheric C fixation and biomass growth in Amazon forests under
102 ambient and eCO₂ conditions (Fleischer *et al.*, 2019). Despite these developments, data to underpin them and
103 their projections, particularly for the tropics, is sparse and remains challenging particularly for the Amazon
104 forest (Reed *et al.*, 2015; Jiang *et al.*, 2019). Moreover, due to the lack of detailed measurements, the P-related
105 processes such as ad/desorption and uptake represented in these models are under-constrained and likely
106 oversimplified, thus the future predictions of Amazon forest responses to eCO₂ and climate change are
107 uncertain. To fill this gap, in this study, we will use data collected as part of the Amazon Fertilization
108 Experiment (AFEX), the first project that focuses on experimental soil nutrient manipulation in the Amazon,
109 with a comprehensive data collection program covering plant ecophysiology, C stocks and fluxes, soil processes
110 including P stocks.

111
112 Here, we describe the implementation of the terrestrial P cycle in the Joint UK Land Environment Simulator
113 (JULES) (Clark *et al.*, 2011), the land component of the UK Earth System Model (UKESM), following the prior
114 N cycle development (Wiltshire *et al.*, 2021). The model (JULES-CNP) is parameterized and then evaluated
115 using AFEX data and from other sites in central Amazonia. AFEX provides the required input data on key plant
116 and soil P pools. To test the model, we followed the protocol of Fleischer *et al.*, (2019), to predict nutrient
117 limitations on land biogeochemistry under ambient and eCO₂. Predictions of the CO₂ fertilization effect in
118 JULES-CNP are compared to those in current versions of the model with coupled C and N cycles (JULES-CN)
119 and with C cycle only (JULES-C).

120
121

122 2. Material and methods

123

124 2.1 JULES

125

126 JULES is a process-based model that integrates water, energy, C cycling (JULES-C) (Clark *et al.*, 2011) and N
127 cycling (JULES-CN) (Wiltshire *et al.*, 2021) between the atmosphere, vegetation and soil (Best *et al.*, 2011;
128 Clark *et al.*, 2011). Vegetation dynamics are represented in JULES using the TRIFFID model, using nine
129 distinct plant functional types (PFTs) (tropical and temperate broadleaf evergreen trees, broadleaf deciduous
130 trees, needle-leaf evergreen and deciduous trees, C3 and C4 grasses, and evergreen and deciduous shrubs), as
131 well as height competition (Harper *et al.*, 2016). JULES simulates Gross Primary Productivity (GPP) based on a
132 coupled photosynthesis and water balance scheme, from which autotrophic respiration for each living tissue
133 (leaf, wood, root) is subtracted to estimate NPP. NPP is then allocated to increase tissue C stocks and to spread,
134 i.e., expand the fractional coverage of the PFT. The resultant PFT fractional coverages depend in addition on
135 competition across PFTs for resources, e.g., light. Tissue turnover and vegetation mortality add C into the litter
136 pools. Representation of soil organic C (SOC) follows the RothC equations (Jenkinson *et al.*, 1990; Jenkinson
137 and Coleman, 2008) defining four C pools: decomposable plant material (DPM) and resistant plant material
138 (RPM), which receive direct input from litterfall, and microbial biomass (BIO) and humified material (HUM)
139 which receive a fraction of decomposed C from DPM and RPM which is not released to the atmosphere. The
140 limitation of N on SOC is applied to the vegetation and soil components using a dynamic C:N ratio to modify
141 the mineralization and immobilization processes as described in Wiltshire *et al.*, (2021). Note that the soil
142 component of JULES-CN can be run either as a single box model or vertically resolved over soil depth (JULES-
143 CNlayered), and in this paper we build upon the vertically resolved version described in Wiltshire *et al.* (2021).

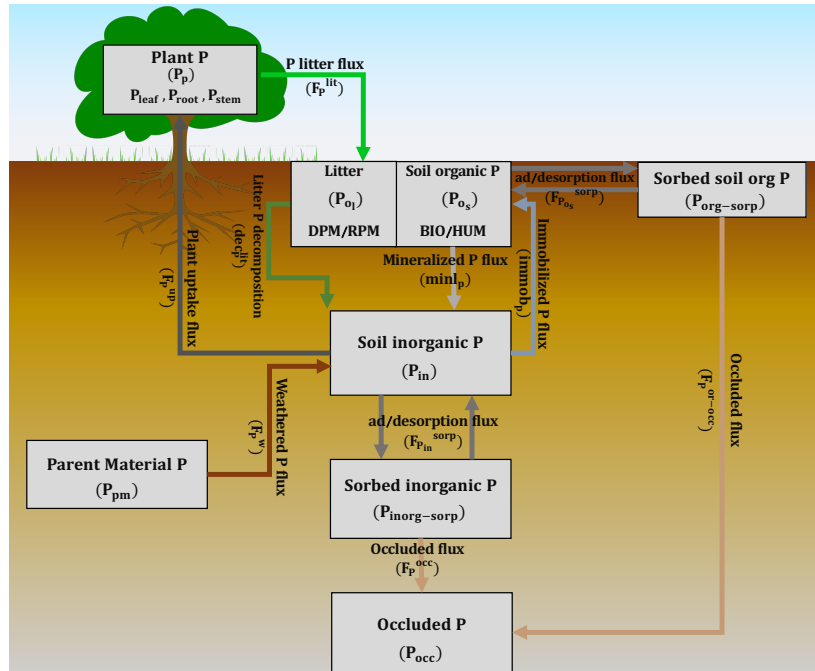
144

145 2.2 JULES-CNP

146

147 JULES-CNP includes the representation of the P cycle in JULES version (vn5.5). It includes P fluxes within the
148 vegetation and soil components, and the specification of P pools and processes related to P cycling within the
149 soil column (Figure.1). A parent material pool is introduced to consider the input of weathered P. The adsorbed,
150 desorbed and occluded fractions of P for both organic and inorganic P are also represented. However, except for
151 parent material and occluded P pools, all other pools are estimated at each soil layer. The description of changes
152 in pools and associated relative fluxes are explained in detail in the next sections.

153



154
 155 **Figure 1-** JULES CNP model scheme
 156

157 **2.2.1 P pools**
 158

159 JULES represents eight P pools comprising organic and inorganic P: in plant P (P_p) and soil pools (in each soil
 160 layer (n): litter P (P_{O_l}), soil organic P (P_{O_s}), soil inorganic P (P_{in}), organic sorbed ($P_{org-sorp}$), inorganic sorbed
 161 ($P_{inorg-sorp}$) and occluded (P_{occ}) P comprised of both organic and inorganic P. All pools are in units of kg P m^{-2}
 162 (Fig 1, Tables 1 and 2).
 163

164 Plant P pool is composed of leaf (P_{leaf}), fine root (P_{root}) and stem together with coarse root (P_{stem}), which are
 165 related to their associated C pools (C_{leaf} , C_{root} , C_{stem}) in (kg C m^{-2}) and C to P ratios ($C:P_{leaf}$, $C:P_{root}$, $C:P_{stem}$)
 166 as follows:
 167

168
$$P_{leaf} = \frac{C_{leaf}}{C:P_{leaf}} \quad (\text{eq.1})$$

169
 170
$$P_{root} = \frac{C_{root}}{C:P_{root}} \quad (\text{eq.2})$$

171
 172
$$P_{stem} = \frac{C_{stem}}{C:P_{stem}} \quad (\text{eq.3})$$

173
 174 Therefore, the plant P pool (P_p) is the sum of all vegetation P pools as follows:
 175

176
$$P_p = P_{leaf} + P_{root} + P_{stem} \quad (\text{eq.4})$$

177 The plant P pool (P_p) is estimated as the difference between the input, plant uptake F_p^{up} (eq.21) and output of
 178 this pool, plant litter flux F_p^{lit} (eq.23), with both fluxes expressed in $\text{kg P m}^{-2} \text{ yr}^{-1}$ as follows:
 179

180
$$\frac{dP_p}{dt} = F_p^{up} - F_p^{lit} \quad (\text{eq.5})$$

181
 182 The litter P pool (P_{O_l}) is estimated as a sum of P_{DPM} and P_{RPM} pools. Each pool (i) is formed by the fluxes of
 183 plant litter input (F_p^{lit}) and the outgoing decomposed P (dec_p^{lit}) both expressed in $\text{kg P m}^{-2} \text{ yr}^{-1}$ (eq.23).



184 Furthermore, the plant litter input is modified based on the plant type material ratio α (in order to distribute the
 185 litter input based on the DPM/RPM fraction) as follows:

$$187 \frac{dP_{DPM}}{dt} = F_{P_n}^{lit} \times \alpha - dec_{P_{i,n}} \quad (\text{eq.6})$$

$$189 \frac{dP_{RPM}}{dt} = F_{P_n}^{lit} \times (1 - \alpha) - dec_{P_{i,n}} \quad (\text{eq.7})$$

$$191 dP_{O_l} = \sum_{n=1}^N P_{DPM_n} + \sum_{n=1}^N P_{RPM_n} \quad (\text{eq.8})$$

192
 193 The soil organic pool (P_{O_s}) is represented as the sum of P_{BIO} and P_{HUM} . These pools are estimated from the
 194 difference between P inputs from immobilized ($immob_{p_i}$) and desorbed P $F_{P_{O_s}}^{desorp}$ and P outputs from
 195 mineralized ($minl_{p_i}$), and adsorbed P fluxes ($F_{P_{O_s}}^{sorp}$) (adsorption: eq. 34 and desorption: eq.35) with all
 196 fluxes expressed in kg P m⁻² yr⁻¹ as follows:

$$198 \frac{dP_{BIO}}{dt} = 0.46 \times immob_{p_i} + F_{P_{O_s,i,n}}^{desorp} - minl_{p_i} - F_{P_{O_s,i,n}}^{sorp} \quad (\text{eq.9})$$

$$200 \frac{dP_{HUM}}{dt} = 0.54 \times immob_{p_i} + F_{P_{O_s,i,n}}^{desorp} - minl_{p_i} - F_{P_{O_s,i,n}}^{sorp} \quad (\text{eq.10})$$

$$202 dP_{O_s} = \sum_{n=1}^N P_{BIO_n} + \sum_{n=1}^N P_{HUM_n} \quad (\text{eq.11})$$

203
 204
 205 The inorganic sorbed P pool ($P_{inorg-sorp}$) is represented as the difference between the input flux of inorganic
 206 sorption ($F_{P_{in}}^{sorp}$) and output fluxes of inorganic desorption ($F_{P_{in}}^{de-sorp}$) and occluded P ($F_{P_n}^{occ}$), with all
 207 fluxes expressed in kg P m⁻² yr⁻¹ as follows:

$$209 \frac{dP_{inorg-sorp}}{dt} = \sum_{n=1}^N F_{P_{in,n}}^{sorp} - \sum_{n=1}^N F_{P_{in,n}}^{de-sorp} - \sum_{n=1}^N F_{P_n}^{occ} \quad (\text{eq.12})$$

210
 211 The occluded (P_{occ}) P pool is represented as the sum of input fluxes of occluded P from both organic ($F_{P_n}^{or-occ}$)
 212 and inorganic P pools ($F_{P_n}^{occ}$) expressed in kg P m⁻² yr⁻¹, as follows:

$$214 \frac{dP_{occ}}{dt} = \sum_{n=1}^N F_{P_n}^{occ} + \sum_{n=1}^N F_{P_n}^{or-occ} \quad (\text{eq.13})$$

215
 216 The organic sorbed P pool ($P_{org-sorp}$) is represented as the difference between the input flux of organic sorption
 217 ($F_{P_{O_s,n}}^{sorp}$) and output fluxes of organic desorption ($F_{P_{O_s,n}}^{de-sorp}$) and occluded P ($F_{P_n}^{occ}$), with all fluxes
 218 expressed in kg P m⁻² yr⁻¹ as follows:

$$220 \frac{dP_{org-sorp}}{dt} = \sum_{n=1}^N F_{P_{O_s,n}}^{sorp} - \sum_{n=1}^N F_{P_{O_s,n}}^{de-sorp} - \sum_{n=1}^N F_{P_n}^{or-occ} \quad (\text{eq.14})$$

221
 222 P from parent material (P_{pm}) pool depends on the weathering flux (F_p^w) in kg P m⁻² yr⁻¹ (eq.37) as follows:

$$224 \frac{dP_{pm}}{dt} = - \sum_{n=1}^N F_{P_n}^w \quad (\text{eq.15})$$

226 2.2.2. P fluxes

227
 228 NPP in JULES is calculated as the difference between GPP and autotrophic respiration. In JULES-CNP, GPP,
 229 autotrophic respiration, and NPP represent the potential amount of C, available for tissue growth and spread
 230 assuming no nutrient limitation. The reported NPP in the literature often includes other C fluxes related to the
 231 exudates, volatiles production and non-structural carbohydrates (Chapin *et al.*, 2011; Walker *et al.*, 2021) which
 232 are challenging to measure (Malhi, Doughty and Galbraith, 2011). Therefore, actual Biomass Production (BP),
 233 as defined by Walker *et al.*, (2021), is calculated based on NPP and the availability and costs associated with
 234 procurement of sufficient inorganic N and P for uptake. Hence, if the system is limited by the availability of N
 235 and/or P, BP will be adjusted to match the growth that can be supported with the limited N or P supply, with any



236 excess carbohydrate lost through exudates. The total excess C term (exudates, ψ_t) (kg C m⁻² yr⁻¹) is calculated
 237 as:

$$238 \psi_t = \psi_g + \psi_s \quad (\text{eq.16})$$

240 where ψ_g and ψ_s are the exudates due to growth (g) and spread (s) and are assumed to be rapidly respired by
 241 plants.

242 P limitation is applied on the C litter production similar to the N scheme of JULES (JULES-CN) (Wiltshire *et*
 243 *al.*, 2021). In JULES-CN the N limitation effect on the litter production is captured by estimating the available C
 244 for litter production as a difference between the NPP and exudates (Wiltshire *et al.*, 2021).

245 BP is calculated as the difference between NPP and total exudates:

$$246 \text{BP} = \text{NPP} - \psi_t \quad (\text{eq.17})$$

247 The plant P demand is represented by the sum of demand to sustain growth (ϕ_g) and to sustain vegetation
 248 spreading (to sustain PFT fractional coverage increment) (ϕ_s) and is expressed in (kg P m⁻² yr⁻¹), as follows:

$$249 \phi_t = \phi_g + \phi_s \quad (\text{eq.18})$$

$$250 \phi_g = \varepsilon_{pc} \left(\Pi_c - \frac{dc}{dt} - \psi_g \right) \quad (\text{eq.19})$$

$$251 \phi_s = \varepsilon_{pc} \left(\Pi_c - \frac{dc}{dt} - \psi_s \right) \quad (\text{eq.20})$$

252 where ε_{pc} is plant P:C ratio, Π_c is the NPP (kg C m⁻² yr⁻¹), ψ_g are exudates due to the P limitation for plant
 253 growth (kg C m⁻² yr⁻¹) and ψ_s are exudates due to the P limitation for vegetation spreading (kg C m⁻² yr⁻¹).

254 Plant P uptake (F_p^{up}) is estimated based on the P demand for growth and spreading (ϕ_t) and the root uptake
 255 capacity (u^{max}) (kg P kg⁻¹ C yr⁻¹), as follows:

$$256 F_p^{up} = \begin{cases} \phi_t & \phi_t \leq u^{max} \\ u^{max} & \phi_t > u^{max} \end{cases} \quad (\text{eq.21})$$

257 The plant P uptake (F_p^{up}) varies spatially depending on the root uptake capacity (u^{max}). Therefore, in regions
 258 with limited P supply, the plant P uptake is limited to the u^{max} and consequently impacts the exudates and BP.
 259 The root uptake capacity depends on the maximum root uptake capacity (v_{max}) (kg P kg⁻¹ C yr⁻¹), root depth
 260 (d_{root}), the concentration of inorganic p at different soil depths (P_{in}), and a half saturation term at which half of
 261 the maximum uptake capacity is reached using inorganic p at different soil depths (P_{in}), a scaling uptake ratio
 262 (K_p) (μmol P l⁻¹), unit conversion (C_f) (1 kg P⁻¹), and soil moisture (θ) (l m⁻²), as follows:

$$263 u^{max} = v_{max} \times d_{root} \times \sum_{n=1}^N P_{in_n} \times \left(\frac{1}{\sum_{n=1}^N P_{in_n} + c_f \times K_p \times \theta_n} \right) \quad (\text{eq.22})$$

264 The litter production of P ($F_{P_n}^{lit}$) is calculated based on the litter flux of C (kg C m⁻² yr⁻¹) using leaf, root and
 265 wood turnovers (yr⁻¹), and through the vegetation dynamics due to large-scale disturbance and litter production
 266 density, as follows:

$$267 F_{P_n}^{lit} = (1 - \lambda_{leaf}) \gamma_{leaf} C_{leaf} \times \varepsilon_{pc-leaf} + (1 - \lambda_{root}) \gamma_{root} C_{root} \times \varepsilon_{pc-root} + \gamma_{wood} C_{wood} \times \varepsilon_{pc-root} \quad (\text{eq.23})$$

268 where λ is the leaf and root P re-translocation coefficient (Zaehle and Friend, 2010) and γ is a temperature
 269 dependent turnover rate representing the phenological state (Clark *et al.*, 2011) and respective C:P ratios.



290 The decomposition of litter (dec^{lit}) depends on soil respiration (R) (kg C m⁻² yr⁻¹), the litter C:P ratio (ϵ_{cp}) at
 291 each soil layer (n) as follows:

$$292 \quad 293 \quad dec_p^{lit} = \frac{\sum_{n=1}^N R_n}{\epsilon_{cp}} \quad (eq.24)$$

294 where the C:P ratio is calculated based on litter C pool (DPM and RPM) (lit^C) (kg C m⁻² yr⁻¹) and litter P pool
 296 (P_{O_i}) as follows:

$$297 \quad 298 \quad \epsilon_{cp} = \frac{\sum_{n=1}^N lit_n^C}{P_{O_{i_n}}} \quad (eq.25)$$

299 The mineralized ($minl_p$) and immobilized ($immob_p$) P fluxes are calculated based on C mineralization and
 300 immobilization, C:P ratios (ϵ_{cp}) of plant (i) (DPM/RPM) and soil (HUM/BIO), soil pool potential respiration
 302 (R_{p_i}) (kg C m⁻² yr⁻¹) and the respiration partitioning fraction ($resp_frac$) as follows:

$$303 \quad 304 \quad minl_p = \frac{\sum_{n=1}^N R_{p_{i_n}}}{\epsilon_{cp_i}} \quad (eq.26)$$

$$305 \quad 306 \quad immob_p = \frac{\sum_{n=1}^N R_{i_n} \times resp_frac}{\epsilon_{cp_{soil}}} \quad (eq.27)$$

307 However, the soil pool potential respiration for the plant pools (DPM/RPM) is further modified based on the
 308 litter decomposition rate modifier (F_{p_n}) as follows:

$$309 \quad 310 \quad 311 \quad R_{i_n} = R_{p_{i_n}} \times F_{p_n} \quad (eq.28)$$

312 where the F_{p_n} is estimated based on the soil pool (BIO/HUM) mineralization and immobilization, soil inorganic
 314 P and plant pools (DPM/RPM) demand as follows:

$$315 \quad 316 \quad F_{p_n} = \frac{(minl_{p-BIO_n} + minl_{p-HUM_n} - immob_{p-BIO_n} - immob_{p-HUM_n}) + P_{inorg_n}}{DEM_{DPM_n} + DEM_{RPM_n}} \quad (eq.29)$$

317 The plant pool demand ($DEM_{k,n}$) is estimated based on the potential mineralization ($minl_{p-pot}$) and
 318 immobilization ($immob_{p-pot}$) of plant pools (k) as follows:

$$319 \quad 320 \quad 321 \quad DEM_{k,n} = immob_{p-pot,k} - minl_{p-pot,k} \quad (eq.30)$$

322 The fluxes of adsorption ($F_{p_{in_n}}^{sorp}$) and desorption ($F_{p_{in_n}}^{desorp}$) of inorganic P in kg P m⁻² yr⁻¹ are calculated
 324 based on soil inorganic (P_{in_n}) and sorbed inorganic ($P_{inorg-sorbed_n}$) P pools and inorganic adsorption
 325 ($K_{sorp-in}$), desorption ($K_{desorp-in}$) coefficients (kg P m⁻² yr⁻¹) and maximum sorbed inorganic (P_{in-max}) (kg P
 326 m⁻²) as follows:

$$327 \quad 328 \quad F_{p_{in_n}}^{sorp} = P_{in_n} \times K_{sorp-in} \times \frac{(P_{in-max_n} - P_{inorg-sorbed_n})}{P_{in-max_n}} \quad (eq.31)$$

$$329 \quad 330 \quad F_{p_{in_n}}^{desorp} = P_{inorg-sorbed_n} \times K_{desorp-in} \quad (eq.32)$$

331
 332
 333 The occluded inorganic p flux is calculated based on sorbed inorganic P pool and P occlusion rate (K_{occ}) (kg P
 334 m⁻² yr⁻¹) as follows:

$$335 \quad 336 \quad 337 \quad F_{p_n}^{occ} = P_{inorg-sorbed_n} \times K_{occ} \quad (eq.33)$$

338
 339 The fluxes of adsorption and desorption of organic P are calculated based on soil organic and sorbed organic P
 340 pools and organic adsorption ($K_{sorp-or}$) (kg P m⁻² yr⁻¹), desorption ($K_{desorp-or}$) coefficients (kg P m⁻² yr⁻¹) and



341 maximum sorbed organic ($P_{org-max}$) (which corresponds to the sorbed soil P saturation, thus modifying the
 342 sorption rate respectively) (kg P m^{-2}) as follows:
 343

$$344 \quad F_{P_{OS_n}}^{sorp} = P_{OS_n} \times K_{sorp-or} \times \frac{(P_{or-max_n} - P_{org-sorbed_n})}{P_{or-max_n}} \quad (\text{eq.34})$$

$$345 \quad F_{P_{OS_n}}^{desorp} = P_{org-sorbed_n} \times K_{desorp-or} \quad (\text{eq.35})$$

347 The occluded organic p flux ($F_{P_n}^{or-occ}$) ($\text{kg P m}^{-2} \text{ yr}^{-1}$) is calculated based on sorbed organic P pool
 348 ($P_{org-sorbed_n}$) and P occlude rate (K_{occ}) ($\text{kg P m}^{-2} \text{ yr}^{-1}$) as follows:
 349

$$350 \quad F_{P_n}^{or-occ} = P_{org-sorbed_n} \times K_{occ} \quad (\text{eq.36})$$

352 The p flux from weathered parent material is calculated based on amount of P in the parent material (P_{pm}) and P
 353 weathering rate (K_w) ($\text{kg P m}^{-2} \text{ yr}^{-1}$) as follows:
 354

$$355 \quad F_{P_n}^w = P_{pm_n} \times K_w \quad (\text{eq.37})$$

357 P diffusion between soil layers (F_{D_n}) expressed in ($\text{kg P m}^{-2} \text{ yr}^{-1}$) is calculated following Fick's second law and
 358 it is a function of the diffusion coefficient (Dz) in $\text{m}^2 \text{ s}^{-1}$, the concentration of inorganic P at different soil depths
 359 (P_{in}) in kg P m^{-2} , the distance (z) between the midpoints of soil layers in metres and seconds to year unit
 360 conversion (Yr):
 361

$$362 \quad F_{D_n} = \frac{\partial}{\partial z} (D_{zn} \frac{\partial P_{zn}}{\partial z}) \times Yr \quad (\text{eq.38})$$

364 **Table 1.** Model variables
 365

Variable	Unit	Definition
ψ	$\text{kg C m}^{-2} \text{ yr}^{-1}$	Excess C exudates
\emptyset	$\text{kg P m}^{-2} \text{ yr}^{-1}$	Plant demand for uptake
Π_c	$\text{kg C m}^{-2} \text{ yr}^{-1}$	Plant C uptake
u^{max}	$\text{kg P kg}^{-1} \text{ C yr}^{-1}$	Root uptake capacity
DEM	$\text{kg P m}^{-2} \text{ yr}^{-1}$	Plant pool P demand
dec_p^{lit}	$\text{kg P m}^{-2} \text{ yr}^{-1}$	Litter decomposition
F_D	$\text{kg P m}^{-2} \text{ yr}^{-1}$	Plant diffusion flux
F_p	-	Plant litter decomposition rate modifier
F_p^{lit}	$\text{kg P m}^{-2} \text{ yr}^{-1}$	Plant litter flux
F_p^{up}	$\text{kg P m}^{-2} \text{ yr}^{-1}$	Plant uptake
$F_{P_{OS}}^{sorp}$	$\text{kg P m}^{-2} \text{ yr}^{-1}$	Sorbed organic P flux
$F_{P_{in}}^{sorp}$	$\text{kg P m}^{-2} \text{ yr}^{-1}$	Sorbed inorganic P flux
F_p^{occ}	$\text{kg P m}^{-2} \text{ yr}^{-1}$	Occluded inorganic P flux
F_p^{or-occ}	$\text{kg P m}^{-2} \text{ yr}^{-1}$	Occluded organic P flux
F_p^w	$\text{kg P m}^{-2} \text{ yr}^{-1}$	Weathered P flux
$immob_p$	$\text{kg P m}^{-2} \text{ yr}^{-1}$	Immobilized P flux
lit_c	$\text{kg C m}^{-2} \text{ yr}^{-1}$	C litter flux
lit_{frac}	-	Litter fraction
lit_{leaf}	$\text{kg C m}^{-2} \text{ yr}^{-1}$	Leaf litter flux
lit_{root}	$\text{kg C m}^{-2} \text{ yr}^{-1}$	Root litter flux
lit_{wood}	$\text{kg C m}^{-2} \text{ yr}^{-1}$	Woody litter flux
$minl_p$	$\text{kg P m}^{-2} \text{ yr}^{-1}$	Mineralized P flux
P_p	kg P m^{-2}	Plant P pool
P_{O_l}	kg P m^{-2}	Litter organic pool



P_{Os}	kg P m ⁻²	Soil organic pool
P_{in}	kg P m ⁻²	Soil inorganic pool
$P_{inorg-sorp}$	kg P m ⁻²	Soil inorganic sorbed pool
$P_{org-sorp}$	kg P m ⁻²	Soil organic sorbed pool
P_{occ}	kg P m ⁻²	Soil occluded pool
P_{pm}	kg P m ⁻²	Parent material pool
R	kg C m ⁻² yr ⁻¹	Total respiration
R_p	kg C m ⁻² yr ⁻¹	Total potential respiration
R^s	kg C m ⁻² yr ⁻¹	Soil respiration
R_d	kg C m ⁻² yr ⁻¹	Leaf dark respiration
T_{ref}	K	Soil reference temperature
T_s	K	Soil temperature
Veg_c	kg C m ⁻²	Sum of biomass
z	m	Soil depth

366
 367

Table 2. P Model parameters

Parameter	Value	Unit	Eq.	Description	Source
α	PFT dependent	-	6	Plant type material ratio	(Clark <i>et al.</i> , 2011)
f_{dr}	0.005	-	41	Respiration scale factor	Calibrated
ϵ_{cp}	1299.6	-	27	C:P ratio	(Fleischer <i>et al.</i> , 2019)
v_{max}	PFT dependent	kg P kg ⁻¹ C yr ⁻¹	22	Maximum root uptake capacity	(Goll <i>et al.</i> , 2017)
d_{root}	PFT dependent	-	22	Root fraction in each soil layer per PFT	(Clark <i>et al.</i> , 2011)
c_f	-	1 kg P ⁻¹	22	Conversion factor	(Goll <i>et al.</i> , 2017)
D_z	Depth dependent	m ² s ⁻¹	38	Diffusion coefficient	(Burke <i>et al.</i> , 2017)
K_{occ}	1.2×10 ⁻⁵	yr ⁻¹	33,36	P occlusion rate	(Yang <i>et al.</i> , 2014)
K_p	PFT dependent	kg P l ⁻¹	22	Scaling uptake ratio	Calibrated
$K_{sorp-in}$	0.0054	kg P m ⁻² yr ⁻¹	31	Inorganic P adsorption coefficient	Calibrated (Hou <i>et al.</i> , 2019)
$K_{sorp-or}$	0.00054	kg P m ⁻² yr ⁻¹	34	Organic P adsorption coefficient	Calibrated
K_{in-max}	0.0075	kg P m ⁻² yr ⁻¹	31	Maximum sorbed inorganic P	AFEX
K_{or-max}	0.0042	kg P m ⁻² yr ⁻¹	34	Maximum sorbed organic P	AFEX
K_w	3×10 ⁻⁶	kg P m ⁻² yr ⁻¹	37	P weathering rate	(Wang <i>et al.</i> , 2010)
$resp_frac$	Pool dependent	kg C m ⁻² yr ⁻¹	27	Respiration fraction	(Clark <i>et al.</i> , 2011)

368
 369
 370
 371
 372
 373
 374
 375
 376
 377
 378
 379
 380
 381
 382
 383
 384
 385
 386
 387
 388

2.3 Study sites

We apply JULES C, CN and CNP to a well-studied site in central Amazonia, where the K34 eddy covariance tower is located (Araújo *et al.*, 2002). This is the main lowland tropical forest site maintained by the National Institute for Amazon Research (INPA). Research at this site focuses on pre-experimental, plot, and full-scale long-term projects, combining experimental approaches (Keller *et al.*, 2004; Malhi *et al.*, 2009) with modelling (Lapola and Norby, 2014). Moreover, a recent manipulation experiment at this site provides an opportunity for future model testing under P fertilization. The K34 site has very similar forest, geomorphology, soil chemistry and species composition to the AFEX site, where the nutrient manipulation experiment takes place and we used the control measurements for model evaluation (Lugli *et al.*, 2021). The average reported annual precipitation is 2431 (mm yr⁻¹), with a monthly range of 95 to 304 (mm month⁻¹), and averaged temperature is 26°C (Araújo *et al.*, 2002). Moreover, the soil class at this site is Geric Ferrosol with a high clay content and weathering activities (Malhi *et al.*, 2004). The AFEX site has a similar condition to K34 site with a dominant old growth vegetation and a very low P content (Lugli *et al.*, 2021).



389 2.4 Model parameterisation, calibration and evaluation

390

391 We use observations from the four control plots of the Amazon Fertilization Experiment to parameterise,
392 calibrate and evaluate different processes in JULES (Table 3). The observations were collected at 4 soil depths
393 and processed using the Hedley sequential fractionation (Hedley, Stewart and Chauhan, 1982; Quesada *et al.*,
394 2010). Observed Leaf Mass per Area (LMA) leaf N and leaf P estimated from fresh leaves were used as input
395 parameters to JULES to estimate photosynthetic capacity and respiration parameters. JULES v1.5 estimates
396 V_{cmax} ($\mu\text{mol m}^{-2} \text{s}^{-2}$) based on Kattge *et al.* (2009) using foliar N concentrations in area basis, as follows:

397

$$398 V_{\text{cmax}} = v_{\text{int}} + v_{\text{sl}} * n_{\text{leaf}} \quad (\text{eq.39})$$

399

400 where v_{int} is the estimated intercept and v_{sl} is the slope of the linear regression derived for the V_{cmax} estimation.
401 We incorporated an additional P dependency on the estimation of V_{cmax} following Walker *et al.* (2014) as
402 follows:

403

$$404 \ln(V_{\text{cmax}}) = 3.946 + 0.921 \ln(N) + 0.121 \ln(P) + 0.282 \ln(N) \ln(P) \quad (\text{eq.40})$$

405

406 Where N and P are foliar concentrations in area basis.

407

408 Implementation of eq. 40 resulted in higher V_{cmax} than in the original version of JULES. A higher V_{cmax} predicted
409 higher leaf and plant respiration (eq.41). Constrained by observations of NPP and plant respiration at the study
410 site, we modified one of the most uncertain parameters in the description of plant respiration (f_{dr}) (eq.41) which
411 is the scale factor (f_{dr}) for leaf dark respiration (R_d) as follows:

412

$$413 R_d = f_{\text{dr}} V_{\text{cmax}} \quad (\text{eq.41})$$

414

415 The default value for this scale factor is 0.01 (Clark *et al.*, 2011), and for JULES-CNP simulations at our study
416 site it was modified to 0.005.

417 Observations of aboveground biomass were used to calibrate the non PFT dependent allometric relationships in
418 JULES (Clark *et al.* 2011) (eq 42-44) for leaf (\mathcal{L}), root (\mathcal{R}) and stem (\mathcal{W}) C. Specifically, the a_{wt} parameter (eq
419 44) was modified from 0.65 to 1.204 to match better tropical forest allometry:

420

$$421 \mathcal{L} = \sigma_l L_b \quad (\text{eq.42})$$

422

$$422 \mathcal{R} = \mathcal{L} \quad (\text{eq.43})$$

423

$$423 \mathcal{W} = a_{\text{wt}} L_b^{b_{\text{wt}}} \quad (\text{eq.44})$$

424

425 Where σ_l is specific leaf density (kg C m^{-2} per unit LAI), L_b is balanced (or seasonal maximum) leaf area index

426

426 ($\text{m}^2 \text{m}^{-2}$), a_{wt} is allometric coefficient (kg C m^{-2}) and b_{wt} is allometric exponent.

427

428 C:P ratios of leaf and root (measured), and stem (estimated; (Lugli, 2013)) were taken from AFEX and
429 prescribed in JULES to simulate P dynamics in the plant. The following belowground data were used to
430 represent various soil P pools: Resin and bicarbonate inorganic P (inorganic P), organic bicarbonate P (organic
431 P), NaOH organic P (sorbed organic P), NaOH inorganic P (sorbed inorganic P), residual P (occluded P) and
432 HCL P (parent material P) (Table 3). The measurements were collected between 2017 and 2018 under a control
433 treatment. All measurements were conducted at four soil layers (0-5, 5-10, 10-20, 20-30 cm). However, to be
434 consistent with the JULES model soil layer discretization scheme, we defined 4 soil layers (0-10 cm, 10-30 cm,
435 30-100 cm and 100-300 cm) and we used the average between 0 and 30 cm to compare against the measurement
436 from the same depth for model evaluation.

437

438 In order to cap P sorption and uptake capacity, the maximum sorption capacities ($P_{\text{in-max}_n}$, $P_{\text{or-max}_n}$, eq.31 and
439 34) were prescribed using observed sorbed inorganic and organic P. Hence, the maximum sorption capacity
440 defines the equilibrium state of sorbed and free-soil P. Moreover, as the magnitude of changes in the occluded
441 and parent material pools are insignificant over a short-term (20 years) simulation period (Vitousek *et al.*, 1997),
442 these two pools were prescribed using observations for these two pools. Remaining parameters used to describe
443 soil P fluxes (eq.s 22 -38) were prescribed using values from the literature (Table 3).

444

445 We used a combination of data from AFEX and the nearby site K34 for model evaluation of C fluxes (GPP,
446 NPP) and C pools (soil and vegetation C, leaf, root and stem C) (Table 3).

447

448



449 **Table 3.** Observations from AFEX (taken during 2017-2018) and from Manaus site K34 used for model parameterisation
 450 and evaluation

Process	Variables	Purpose of use	Reference and site
C associated	GPP	Evaluation	Fleischer et al., 2019, K34
	NPP	-/-	Fleischer et al., 2019, K34
	Soil C	-/-	Malhi et al., 2009, K34
	CUE	-/-	Malhi et al., 2009, K34
	Veg C	-/-	AFEX project measurements
	Leaf C	-/-	AFEX project measurements
	Stem C	-/-	AFEX project measurements
	Root C	-/-	AFEX project measurements
	LAI	Initialisation	AFEX project measurements
	LMA	Parameterisation	AFEX project measurements
P associated	Resin	Evaluation	AFEX project measurements
	Pi Bic	Evaluation	-/-
	Po Bic	-/-	-/-
	Po NaOH	-/-	-/-
	Pi NaOH	-/-	-/-
	P residual	Parameterisation	-/-
	P HCL	-/-	-/-
	Leaf N	-/-	-/-
	Leaf P	-/-	-/-
	Root P	-/-	-/-
Plant C:P ratio	-/-	-/-	

451

452 2.5 JULES simulations

453

454 JULES was applied at the K34 flux tower site using observed meteorological forcing data from 1999-2019
 455 (Fleischer et al. 2019) at half hourly resolution. The following meteorological variables are needed to drive JULES
 456 (Best *et al.*, 2011): atmospheric specific humidity (kg kg^{-1}), atmospheric temperature (K), air pressure at the
 457 surface (Pa), short and longwave radiation at the surface (W m^{-2}), wind speed (m s^{-1}) and total precipitation (kg
 458 $\text{m}^{-2} \text{s}^{-1}$). Furthermore, the LAI measurements from AFEX were used to initialise the vegetation phenology
 459 module. All soil P pools were initialised with AFEX observations. To reach equilibrium between pools and
 460 fluxes, JULES-CNP was run 1000 times recycling a 20-year climate (1999-2019) and constant present-day CO_2
 461 until reaching steady state (Figure. S1). Finally, the transient run for the period 1999-2019 was then performed
 462 using time-varying observed CO_2 and N deposition. Furthermore, the eCO_2 experiment runs for the period 1999-
 463 2019 was performed using the transient run forcing data. Note that the spin up was performed separately for
 464 three versions of JULES (C/CN/CNP) following the same procedure.

465

466 We evaluate the impact of including a P cycle in JULES using three model configurations (JULES C, CN and
 467 CNP). We apply JULES in all three configurations using present day climate under both ambient CO_2 and
 468 elevated CO_2 (eCO_2). Ambient and eCO_2 were prescribed following Fleischer *et al.*, (2019), with present-day
 469 CO_2 based on global monitoring stations, and a step increase in CO_2 of +200 ppm on the onset of the transient
 470 period (i.e., 1999). However, the comparison period is limited to 2017-18 for which the P measurements are
 471 available.

472

473 We compare simulated C fluxes (GPP, NPP, litterfall C), C stocks (total vegetation, fine root, leaf, wood, soil)
 474 and the CO_2 fertilization effect across model configurations. The CO_2 fertilization effect ($\text{CO}_2_{\text{fert-eff}}$) (eq.45)
 475 is calculated based on simulated vegetation C under ambient ($\text{VegC}(\text{aCO}_2)$) and eCO_2 ($\text{VegC}(\text{eCO}_2)$) as
 476 follows:

477

$$478 \text{CO}_2_{\text{fert-eff}} = \frac{(\text{VegC}(\text{eCO}_2) - \text{VegC}(\text{aCO}_2)) \times 100}{\text{VegC}(\text{aCO}_2)} \quad (\text{eq.45})$$

479

480 Furthermore, the net biomass increases due to CO_2 fertilization effect ($\Delta\text{C}_{\text{veg}}$) is estimated as follows:

481

$$482 \Delta\text{C}_{\text{veg}} = \Delta\text{BP} - \Delta\text{litterfall C} \quad (\text{eq.46})$$



483 We studied the Water Use Efficiency (WUE) (eq. 47), as one of the main indicators of GPP changes (Xiao *et*
 484 *al.*, 2013), and soil moisture (SMCL), as one of the main controllers of maximum uptake capacity (eq. 22), in
 485 order to better understanding the changes in GPP, P demand and uptake as well as exudates fluxes.

486
 487
$$WUE = GPP/Transpiration \quad (\text{eq.47})$$

488
 489 Moreover, we also estimated the Carbon Use Efficiency (CUE) as an indicator of the required C for the growth
 490 (Bradford and Crowther, 2013) as follows:

491
 492
$$CUE = BP/GPP \quad (\text{eq.48})$$

493
 494 We use JULES-CNP to evaluate the extent of P limitation under ambient and eCO₂ at this rainforest site in
 495 Central Amazon. P limitation is represented by the amount of C that is not fixed by plants due to the insufficient
 496 P in the system (exudates) (eq. 22). The exudate flux is highly dependent on the plant P and the overall P
 497 availability to satisfy demand. We also explore the distribution of the inorganic and organic soil P and their
 498 sorbed fraction within the soil layer and under ambient and eCO₂.

499
 500 To test the sensitivity of the P and C related processes to the model P parameters, two sets of simulations were
 501 conducted with modified C:P ratio of the leaf, stem, and root pools. These values were prescribed to vary
 502 between ±50% of the observed values and their effect on C pools (plant and soil C) and fluxes (NPP and
 503 exudates), and P pools (plant, soil, and soil sorbed P) was assessed.

504
 505 Our model evaluation period is limited to years 2017-18 due to the P measurement availability. However, in
 506 order to perform inter-models comparison with 15 models studied by Fleischer *et al.*, (2019) we also studied the
 507 response of GPP, NPP and BP to eCO₂ for both initial (1999) and 15 years periods (between 1999-2013).

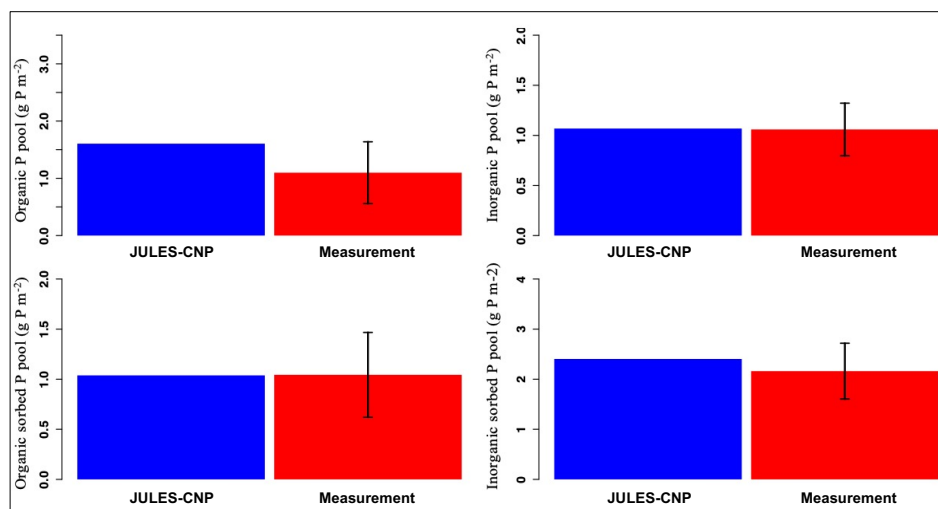
508
 509 **3. Results**

510
 511 **3.1 Model application under ambient CO₂**

512
 513 **3.1.1 Calibration of simulated soil P pools**

514
 515 The maximum sorption capacities (P_{in-max_n} , P_{or-max_n} , eq.31 and 34) were calibrated to the observed P pools.
 516 As a result, JULES-CNP could reproduce the measured soil p pools (Figure. 2 and Table 4). Simulated
 517 inorganic soil P and sorbed organic and inorganic soil P closely matched the observations (Table 5 and Figure.
 518 2). However, simulated organic soil P overestimates the observations by 60 %.

519



520
 521
 522
 523

Figure. 2- Modelled vs measured soil phosphorus pools under ambient CO₂ (for the soil depth of 0-30cm). Black line represents standard deviation



524 **Table 4.** Observed and simulated phosphorus pools and fluxes. Occluded and weathered P pools were prescribed using the
 525 observed values (between period 2017-18).

	Phosphorus pools and fluxes		
	Measured	Modelled Ambient CO ₂	Modelled Elevated CO ₂
Organic P (g P m ⁻²)	1.09±0.53	1.6	1.57
Inorganic P (g P m ⁻²)	1.05±0.33	1.07	0.96
Sorbed organic P (g P m ⁻²)	1.04±0.42	1.04	1.03
Sorbed inorganic P (g P m ⁻²)	2.1±0.55	2.4	2.4
Occluded P (g P m ⁻²)	7.98±2.38	prescribed	prescribed
Weathered P (g P m ⁻²)	0.59±12	prescribed	prescribed
Total vegetation P (g P m ⁻²)	4.15	4.66	5.11
Soil P – 30cm (g P m ⁻²)	13.85	14.7	14.56
Total ecosystem P (g P m ⁻²)	-	35.97	35.97
P litter flux (g P m ⁻² yr ⁻¹)	0.3	0.28	0.29

526
 527
 528
 529
 530
 531
 532
 533
 534
 535
 536
 537
 538
 539
 540
 541
 542
 543
 544

3.1.2 Model evaluation

JULES-CNP could reproduce the plant and soil C pools and fluxes under ambient CO₂ (Figure. 2 and Table 5). Our results show that simulated GPP, is within the range of measurement (3.02 kg C m² yr⁻¹ model vs 3-3.5 kg C m² yr⁻¹ observed, respectively, Table 5).

Simulated NPP, is close to the measured values (NPP: 1.14 - 1.31 observed vs 1.26 modelled kg C m² yr⁻¹) with autotrophic respiration (RESP) also closely following the observations (1.98 observed vs 1.81 modelled kg C m² yr⁻¹). Biomass production is estimated as a difference between NPP and the amount of C which is not fixed by plants due to the insufficient P in the system (exudates) (eq. 22). The exudate flux is highly dependent on the plant P and the overall P availability to satisfy demand (Table 5). Simulated flux of exudates is 0.3 kg C m² yr⁻¹ under ambient CO₂. In JULES-CNP this flux is subtracted from NPP in order to give the BP (eq. 17) (Table 5). Our simulated litterfall overestimates the observations by 32%, however simulated vegetation and its components (fine root, leaf and wood) and soil C stocks match well the observations (Table 5).

Table 5. Observed and simulated carbon pools and fluxes with JULES_CNP (between period 2017-18)

	Carbon pools and fluxes		
	Measured	Modelled Ambient CO ₂	Modelled Elevated CO ₂
GPP (kg C m ² yr ⁻¹)	3.0 – 3.5	3.06	3.9
NPP (kg C m ² yr ⁻¹)	1.14-1.31	1.27	1.77
Plant respiration (kg C m ² yr ⁻¹)	1.98	1.78	2.12
Exudates (kg C m ² yr ⁻¹)	-	0.30	0.81
Biomass Production (kg C m ² yr ⁻¹)	-	0.96	0.94
Litter C flux (kg C m ⁻² yr ⁻¹)	0.69	0.91	0.83
Leaf C (kg C m ⁻²)	0.37	0.38	0.40
Wood C (kg C m ⁻²)	22.01	22.4	24.71
Root C (kg C m ⁻²)	0.37	0.38	0.40
Vegetation C (kg C m ⁻²)	22.75	23.16	25.52
Soil C stock (kg C m ⁻²)	12.7	13.2	12.71
LAI (m ² m ⁻²)	5.6	5.77	6.12

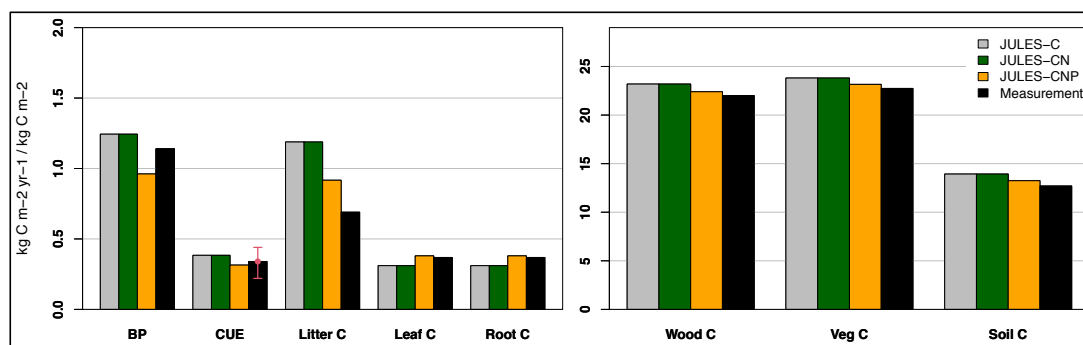
545
 546



547 **3.1.3 Comparison of JULES C, CN and CNP under ambient CO₂**

548
 549
 550
 551
 552
 553
 554
 555
 556
 557
 558
 559
 560
 561
 562
 563

We compare simulated C pools and fluxes from JULES-C, JULES-CN and JULES-CNP (Figure. 3). There is no difference between C stocks and fluxes in simulations from JULES C and CN indicating that there is no N limitation at this tropical site in the CN simulations. However, simulated BP and litter flux of C by JULES C/CN are higher than in JULES-CNP but also overestimate the observations (litter flux of JULES C/CN: 1.18, JULES CNP: 0.91 and obs 0.69 (kg C m⁻² yr⁻¹) and BP of JULES C/CN: 1.24, JULES CNP: 0.96 and obs 1.14-1.31 (kg C m⁻² yr⁻¹), respectively). By including the P cycling in JULES an exudate flux of 0.3 (kg C m⁻² yr⁻¹) is simulated, indicating a 24% P limitation to BP at this site according to JULES CNP, which represents a 29% decrease in BP compared to JULES-C/CN. Consequently, the total vegetation C stock for models without P inclusion is higher than the CNP version (+3% difference) due to the lack of representation of P limitation. The simulated soil C stock in JULES C and JULES CN is also higher than in the CNP version (JULES C/CN: 13.93 vs. JULES CNP: 13.18 (kg C m⁻² yr⁻¹)) and higher than the observations. Moreover, CUE in JULES C/CN (eq.42) is higher than observations and JULES CNP version (JULES C/CN: 0.38 vs. JULES CNP: 0.31, obs: 0.34 ± 0.1 (dimensionless)).

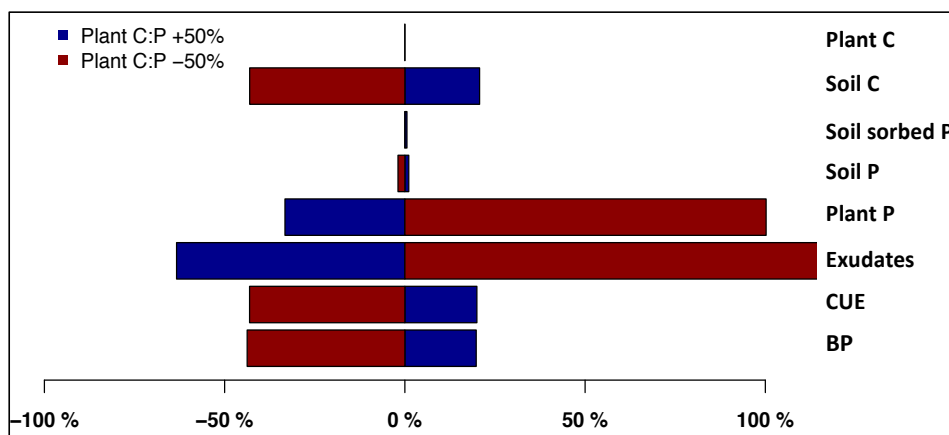


564
 565
 566
 567
 568
 569
 570
 571
 572
 573
 574
 575
 576
 577
 578
 579

Figure. 3- JULES C, CN, CNP modelled vs measured C pools (in kg C m⁻²) and fluxes (in kg C m⁻² yr⁻¹) under ambient CO₂. Note that CUE is unitless.

3.1.4 Model sensitivity to C:P stoichiometry

Model sensitivity to plant C:P stoichiometry was tested at ±50% change from default values. The results indicate that among all the corresponding C and P pools and fluxes, the exudate flux -which determines P limitation to NPP - shows the highest sensitivity to changes in C:P ratios. The decrease of the plant C:P results in a large increase in exudates. This is due to the higher plant P demand as a result of lower plant C:P ratios. Since the total P in the system is lower than the plant demand, higher P limitation is placed on C fixation (decreasing BP) which results in an increase in exudates (Figure. 4) but also causes a decrease in soil C which is a result of the lower fixed C by the plants. Moreover, total soil P shows low sensitivity to changes in plant C:P, and total plant C and soil sorbed P pools show no sensitivity to plant C:P ratios.



580
 581
 582
 583
 584
 585
 586
 587
 588
 589
 590
 591
 592
 593
 594
 595
 596
 597
 598
 599
 600
 601
 602
 603
 604
 605
 606
 607
 608
 609
 610
 611
 612
 613
 614
 615
 616
 617
 618
 619
 620
 621

Figure 4- Model sensitivity test results and corresponding C and P pools and fluxes under ambient CO₂.

3.2 Model application under elevated CO₂

3.2.1 Simulated plant and soil C and P pools and fluxes -JULES CNP: eCO₂ vs ambient CO₂

The eCO₂ simulation using JULES CNP yields a higher GPP compared to the ambient CO₂ (0.83 (kg C m⁻² yr⁻¹) increase), as a result of CO₂ fertilization. Moreover, due to the GPP increase, NPP and RESP follows the same trend and increased compared to ambient CO₂ (NPP: 0.49 and RESP:0.3 (kg C m⁻² yr⁻¹) increase) (Table 5). The total simulated vegetation C pool increases under eCO₂ compared to ambient CO₂ (0.41 kg C m⁻²), hence the estimated plant P (estimated as a fraction of C:P ratios) increases as well (+0.45 (g P m⁻²)) (Fig 6, Table 4). Thus, the simulated plant P demand is higher, and as the total available soil P for uptake is limited, the simulated exudate flux increases to 0.51(kg C m⁻² yr⁻¹). Moreover, despite the higher NPP under eCO₂ compared to simulated NPP under ambient CO₂, due to the substantial increase in simulated exudates, the BP is similar to the ambient CO₂ (2% difference).

The simulated organic soil P under eCO₂ yields close to the ambient CO₂ (1.6 g P m⁻²) (Table 5). This is due to the same parameterization of the output fluxes from this pool for eCO₂ and ambient CO₂. The simulated pool of inorganic P under eCO₂ decreases compared to the ambient CO₂ by 0.11 (g P m⁻²) due to the increased plant P pools and slight increase in uptake (+0.13 %).

However, the simulated sorbed organic and inorganic soil P from eCO₂ are similar to those simulated under the ambient CO₂ which is due to the same parameterizing of sorption function (maximum sorption capacity) from the ambient CO₂ run as explained in calibration section. Moreover, the modelled occluded and weathered soil P yield similar to those in the ambient CO₂ simulation (Table 5) which is due to the same prescribed observational data that was used for this simulation.

3.2.2 Comparison of JULES C, CN and CNP under elevated CO₂

JULES C/CN show higher vegetation and soil C pools, BP and litter flux compared to JULES-CNP: (Table 6, Figure. S2). Under eCO₂, simulated NPP using JULES C-CN is 4.5% higher than JULES CNP and the BP with JULES- C/CN is 96.8% higher than in JULES-CNP which simulates an exudates flux of 0.81 (kg C m⁻² yr⁻¹) equivalent to 46% P limitation under eCO₂. As a result of P limitation and eCO₂, the simulated CO₂ fertilization effect estimated based on changes in biomass under ambient and eCO₂ was reduced from 13% with JULES-C/CN to 10% JULES-CNP. Moreover, the CUE from JULES C/CN is 87.5% higher than the JULES CNP as a result of high P limitation over biomass production.



622 **Table 6.** C pools and fluxes using JULES C/CN and difference in percentage with JULES CNP model under eCO₂. A
 623 positive % means larger respective values simulated with JULES C and JULES CN than with JULES CNP (between period
 624 2017-18).

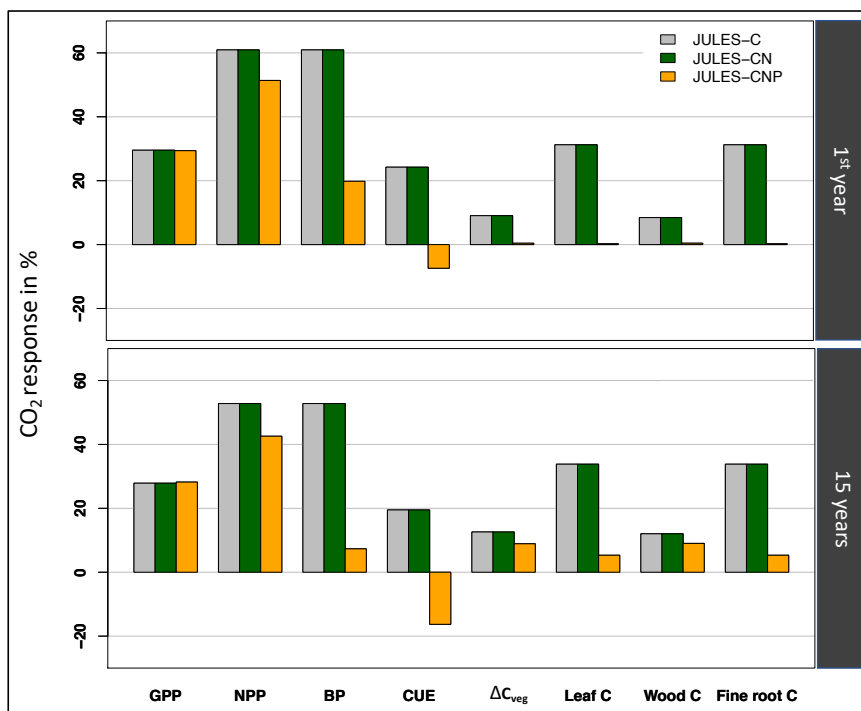
	GPP	NPP	BP	CUE	Litter C	Leaf C	Root C	Wood C	Soil C
JULES C/CN	4.1	1.85	1.85	45%	1.77	0.42	0.42	26.1	19.2
JULES CNP	3.9	1.77	0.94	24%	0.83	0.4	0.4	24.71	12.71
ΔC/CN: CNP	5.1%	4.5%	96.8%	87.5%	113.3%	5%	5%	5%	51.1%

625
 626 **3.2.2.1 Inter-models under elevated CO₂**
 627

628 Following Fleischer *et al.*, (2019), we report the simulated response to eCO₂ for year 1999 (initial: CO₂ effect)
 629 and 1999-2013 (15 years: final effect) which are different than our evaluation period (2017-18). Using JULES C
 630 and JULES CN under eCO₂, simulated GPP and NPP during the 1st year increase by 30% and 61% respectively
 631 and by 28% and 52% after 15 years (Figure. 5). However, using JULES CNP, eCO₂ increases simulated GPP,
 632 NPP and BP responses during the 1st year by 29%,51% and 20% and by 28%, 43% and 7%, after 15 years
 633 respectively.

634
 635 Corresponding simulated CUE during the 1st year and 15 years shows an increase of 24% and 20% in response
 636 to eCO₂ using JULES C/CN respectively. However, using JULES CNP, simulated CUE for the 1st and after 15
 637 years is reduced by 7% and 17% in response to eCO₂.

638
 639 Simulated total biomass (leaf, fine root and wood C) (ΔC_{veg}) using JULES C/CN for the 1st and 15 years of
 640 eCO₂ increases by 9% and 13% respectively. However, using JULES CNP ΔC_{veg} only increases by 0.5% and
 641 9% for 1st and 15 years of eCO₂, respectively.
 642
 643



644
 645 **Figure 5-** Relative effect of eCO₂ on simulated GPP, NPP, BP, CUE, ΔC_{veg}, leaf C, wood C and fine root C, using three
 646 versions of JULES model in 1st (initial response) and 15 years periods (final response).
 647
 648
 649



650 3.3 Plant P Demand, uptake and exudates under ambient and elevated CO₂

651

652 To understand further the CP-cycle dynamics, we studied the monthly averaged plant P demand and the relative
 653 (limited) P uptake (eq. 21) under both ambient and elevated CO₂ conditions (Figure. 6).

654

655 Under ambient CO₂ condition the highest GPP is estimated at 3.5±0.19 kg C m⁻² yr⁻¹ in July and the lowest at
 656 2.06±0.61 kg C m⁻² yr⁻¹ in October (Figure. 6-a). The estimated WUE and SMCL in October is among the lowest
 657 estimated monthly values at 2.3±0.51 kg CO₂/kg H₂O and 526.2±31 kg m⁻² respectively (Figure. 6-c). The
 658 highest P demand is estimated at 0.4±0.02 g P m⁻² yr⁻¹ in July and the lowest demand at 0.2±0.08 g P m⁻² yr⁻¹
 659 in October. Consequently, the highest and lowest uptake (0.32±0.01 and 0.19±0.07 g P m⁻² yr⁻¹, respectively). The
 660 exudates for the highest and lowest GPP and demand periods are estimated at 0.4±15 and 0.04±0.07 kg C m⁻² yr⁻¹,
 661 respectively.

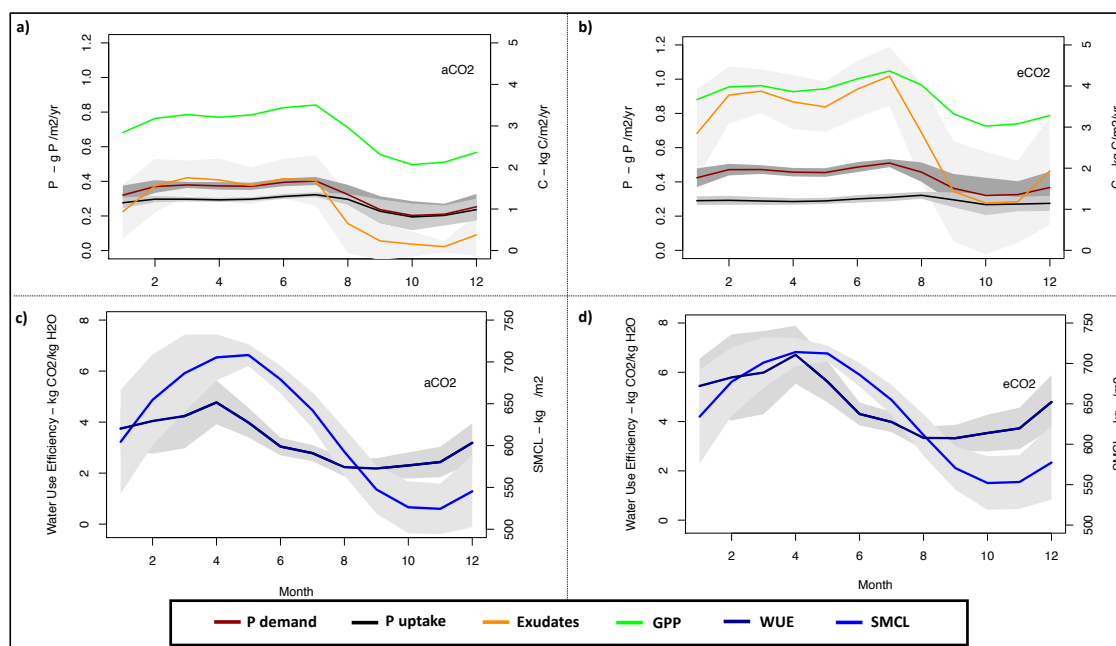
662

663 However, similar to ambient CO₂, under eCO₂ condition the highest estimated GPP is in July at 4.36±0.21 kg C
 664 m⁻² yr⁻¹ and lowest for October 3.02±0.75 kg C m⁻² yr⁻¹ (Figure. 6-b). The estimated WUE and SMCL for the
 665 lowest GPP period is among the lowest monthly estimated values at 3.5±0.74 kg CO₂/kg H₂O and 552±33 kg m⁻²
 666 for October respectively (Figure. 6-d). The highest P demand is estimated for July at 0.51±0.02 g P m⁻² yr⁻¹
 667 with the uptake flux of 0.31±0.02 g P m⁻² yr⁻¹ and the lowest demand is estimated for October at 0.32±0.1 g P m⁻²
 668 yr⁻¹ with the estimated uptake flux of 0.26±0.06 g P m⁻² yr⁻¹. The highest exudate flux is also for July at
 669 1.01±0.17 kg C m⁻² yr⁻¹ and lowest for October 0.27±0.29 kg C m⁻² yr⁻¹, respectively.

670

671 However, despite the P limitation in both eCO₂ and ambient CO₂ conditions, the P uptake flux under eCO₂ is
 672 higher than the ambient CO₂ condition. This is due to the higher WUE and increased soil moisture (SMCL)
 673 (controlling uptake capacity (eq. 22)) under eCO₂ condition, hence more water availability during the dry season
 674 to maintain productivity and critically transport P to the plant (see eq. 22), compared to ambient CO₂ condition
 675 (Figure. 6-c and d).

676



677

678 **Figure. 6-** Simulated monthly plant P demand and uptake (g P m⁻² yr⁻¹), exudates and GPP (kg C m⁻² yr⁻¹) under a) aCO₂ and
 679 b) eCO₂, water use efficiency (g m⁻² yr⁻¹) under c) ambient CO₂ (aCO₂) and d) eCO₂ conditions. The grey area represents the
 680 standard deviation.

681

682

683

684



685 3.4 Soil P pools profile under ambient CO₂ and elevated CO₂

686

687

688

689

690

691

692

693

694

695

696

697

698

699

700

701

702

703

704

705

706

707

708

709

710

711

712

713

714

715

716

717

718

719

720

721

722

723

724

725

726

727

728

729

730

731

732

733

734

735

736

737

738

739

740

741

742

743

We explored the distribution of the inorganic and organic soil P and their sorbed fraction within the soil layers and under different CO₂ conditions (Figure. S3). Both the ambient and eCO₂ simulations have a close inorganic soil P distribution at the topsoil layer (0-30cm) (0.85 vs. 0.9 (g P m⁻²) respectively) as well as similar organic soil P distribution (0.85 vs 0.9 (g P m⁻²) respectively) which is in line with the observational study by Tian *et al.*, (2017).

However, the organic soil P and sorbed forms of inorganic and organic soil P profiles are not changing significantly between different sets due to the similar parameterization of the processes that control these pools (processes which are related to the physical aspects of soils, hence not changing under eCO₂ condition) and the same parameter values used for both ambient and eCO₂ runs.

Moreover, the soil P within 30cm soil depth for ambient and eCO₂ conditions is at 14.7 (g P m⁻²) and 14.56 (g P m⁻²) respectively, and the total ecosystem P for both ambient and eCO₂ conditions is at 35.97 (g P m⁻²).

However, the slightly lower soil P in the eCO₂ condition is due to the higher plant P demand compared to the ambient condition, hence the higher allocated P vegetation (10%) under eCO₂ condition.

704 4. Discussion

705 Studies show the significant role of the tropical forests, and Amazonia in particular, in C uptake and regulating atmospheric CO₂ (Brienen *et al.*, 2015; Phillips *et al.*, 2017). As soil P availability is low in the majority of Amazonia (Quesada *et al.*, 2012), the competition in both plant and soil communities is high (Lloyd *et al.*, 2001). Therefore, the responses of these communities to eCO₂ under P limited conditions are still unclear (Fleischer *et al.*, 2019). Hence, we included the P cycling representation in JULES model to improve the carbon-nutrients feedbacks and study the responses under ambient and eCO₂ conditions in a well-documented low fertility site which is representative of about 60% of Amazon soils (Quesada *et al.*, 2010). Our new developments include in detail all the major P processes in both plant and soil pools and can be applied to the Amazon region using existing soil (Quesada *et al.*, 2011) and foliar structural and nutrient (Fyllas *et al.*, 2009) data for parameterisation.

717 4.1. Evaluation of model performance against observations

718 JULES-CNP could reproduce the magnitude of plant and different forms of soil P pools and fluxes. The relative distribution of total organic P, total inorganic P and residue P fractions of total P in soils under Brazilian Eucalyptus plantations (Costa *et al.*, 2016) shows inorganic P fraction of 28% from total soil P which is close to our estimation of 24% and organic P fraction of 30% from total soil P which is higher than our estimated fraction of 18%. Thus, we may need to improve the process representation or parameters that control the organic P concentration, such as litter flux and decomposition, soil organic P mineralization, and immobilization in the future.

726 Our estimated maximum P uptake, which represents the actual available P for plant uptake (Wang and Goll, 2021), for both ambient and eCO₂ conditions, is highly correlated with the plant P demand ($R^2 = 0.96$ and 0.52 respectively). The plant P demand depends on the GPP changes which are reflected by the WUE (Hatfield and Dold, 2019). Hence, under ambient CO₂, JULES CNP simulates lower GPP and plant P demand during the dry season than during the wet season. Sufficient P uptake during these periods results in the lowest P limitation, thus the lowest simulated exudates. Nevertheless, under eCO₂ the same pattern is simulated but a higher availability of soil P due to the stomatal closure in the dry season. Hence, due to the plant's more efficient water usage, the soil moisture in the dry season is higher (Xu *et al.*, 2016) which impacts our capped P uptake flux (eq. 22) and increases the uptake capacity respectively.

736 Overall, JULES-CNP reproduced the observed C pools and fluxes which are in the acceptable ranges compared to the measurements. However, using the JULES default V_{cmax} estimation method (eq. 39), the model slightly underestimates the total GPP (2.9 kg C m⁻² yr⁻¹ vs. 3-3.5 kg C m⁻² yr⁻¹). Therefore, in this version of the model, we used the improved V_{cmax} estimation method based on N and P (eq. 40) which resulted a final estimated GPP closer to the measurements (3.06 kg C m⁻² yr⁻¹).



744 Our results show an increase in GPP (21%) in response to eCO₂ which is higher than the average increase of
745 GPP reported in mature eucalyptus forests (11%), also growing under low P soils at the free air CO₂ enrichment
746 experiment (EucFACE) facility in Australia (Jiang *et al.*, 2020). This can be related to the lower decrease of
747 biomass growth response estimated by JULES-CNP (-3%) compared to the measurements from mature forests
748 (-8%) (Ellsworth *et al.*, 2017), due to the P limitation which showed to impact the above-ground biomass
749 growth response in mature forests (Körner *et al.*, 2005; Ryan, 2013; Klein *et al.*, 2016).
750

751 In order to estimate the biomass production (BP), we deducted the exudates fluxes from the NPP. Using JULES
752 C/CN models our estimated biomass productivity enhancement due to eCO₂ (49%) is in the middle range of the
753 reported various studies from different biomes by Walker *et al.*, (2021). Moreover, our estimated difference of
754 BP between ambient and eCO₂ conditions (2%) is close to the estimated difference for mature forests (3%)
755 (Jiang *et al.*, 2020).
756

757 A global estimation for tropical forests using CASACNP model which includes N and P limitations on
758 terrestrial C cycling, shows that NPP is reduced by 20% on average due to the insufficient P availability (Wang,
759 Law and Pak, 2010) which is close to our estimated P limitation of 24%. This finding is in line with
760 experimental study that shows a strong correlation between the total NPP and the soil available P (Aragão *et al.*,
761 2009). Nevertheless, our model show that the P limitation mimics the same response to the CO₂ fertilization
762 similar to sites in pool soils (see ZAR-01 site in Aragão *et al.*, (2009)). The estimated decrease of NPP in
763 response to eCO₂ as a result of P limitation is in line with the findings from CLM-CNP model at five tropical
764 forests (Yang *et al.*, 2014) which indicates the CO₂ fertilization dependency on the processes that affect P
765 availability or uptake.
766

767 Our estimated CUE (0.31) is close to the estimation by Jing *et al.* (2020) for mature forests (0.31±0.03), as well
768 as to the measurement for our study site (0.34 ±0.1). There is currently a lack of representation of stand age in
769 JULES-CNP which can significantly change this ratio (e.g. mature trees are less responsive to the nutrient
770 limitations) (De Lucia *et al.*, 2007; Norby *et al.*, 2016). However, a recent development of Robust Ecosystem
771 Demography (RED) model into JULES (Argles *et al.*, 2020) and its integration into JULES-CNP in the future
772 can resolve this issue.
773

774 4.2. Inter-models comparison

775
776 The comparison of simulated GPP enhancement across JULES versions for the 1st year is within the middle
777 range of the 1st year CO₂ responses of the C/CN models studied by Fleischer *et al.*, (2019) evaluating simulated
778 eCO₂ effects at a site in Manaus using the same meteorological forcing and methodology used in this study for
779 a range of DGVM's. However, comparison for 15 years of eCO₂, shows that the simulated response with
780 JULES CNP is on the higher end of Fleischer *et al.*, (2019) study which is due to the higher estimated biomass
781 growth by JULES CNP (Table S1). Similarly, using JULES CNP our estimated GPP enhancement is on the
782 higher end of model estimations in Fleischer *et al.*, (2019). Moreover, comparing the GPP responses between
783 different versions of (JULES C/CN and CNP), the JULES CNP shows a slightly higher response to CO₂
784 fertilization associated with the higher WUE changes (Xiao *et al.*, 2013) (Figure. S4). This is due to the higher
785 sensitivity of the plant to water availability than the P availability in the P limited system (He and Dijkstra,
786 2014). Hence, under eCO₂ due to water-saving strategy of plants and stomatal closure (Medlyn *et al.*, 2016),
787 simulated transpiration is decreased (Sampaio *et al.*, 2021) and photosynthesis is enhanced compared ambient
788 CO₂.
789

790 To that end, the monthly changes of WUE in JULES CNP are highly correlated to the GPP, hence the lowest
791 and highest WUE follow the same periods as GPP similar to responses captured with models studied by
792 Fleischer *et al.*, (2019) (Table. S1).
793

794 Our estimated NPP enhancement using JULES C/CN models for both 1st and 15 years period is within the
795 middle range of the models in Fleischer *et al.*, (2019). Nevertheless, JULES CNP response of BP is in the lower
796 band of the CNP models by Fleischer *et al.*, (2019) and close to the estimations from CABLE (Haverd *et al.*,
797 2018) and ORCHIDEE (Goll *et al.*, 2017) models, which may be due to the similar representation of P processes
798 and limitation between these models. However, our results show a 29% decrease in NPP using JULES-CNP
799 compared to JULES-C/CN which is smaller than the differences between the CLM-CNP and CLM-CN versions
800 (51% decrease) (Yang *et al.*, 2014). The lower estimated decrease in JULES highlights the need to further study
801 the fully corresponding plant C pools and fluxes to the changes in soil and plant P. Therefore, future work
802 should be focused on the improvement of the total P availability and the plant C feedbacks. Moreover, there are



803 other environmental factors such as temperature which shows a possible impact on the CO₂ elevation and the
804 changes of NPP (Baig *et al.*, 2015) which needs further improvement in our model.
805 The CUE estimations of 1st year and 15 years response to CO₂ elevation from JULES C/CN are in the middle
806 range of C/CN models in Fleischer *et al.*, (2019). However, the estimated CUE using JULES CNP for 1st and 15
807 years are in the low range of CNP models reported by Fleischer *et al.*, (2019) which is due to the same reason
808 discussed for NPP comparison.
809

810 Finally, our estimated total biomass enhancement (ΔC_{veg}) using JULES C/CN for the 1st and 15 years are in the
811 middle range of C/CN models from Fleischer *et al.*, (2019) and in lower range of CNP models from Fleischer *et*
812 *al.*, (2019) using JULES CNP. Nevertheless, while JULES-CNP includes the trait-based parameters (Harper *et*
813 *al.*, 2016), other functions such as flexible C allocation and spatial variation of biomass turnover are still
814 missing and future model improvement should be focused on their inclusion.
815

816

817 5. Conclusion

818

819 Land ecosystems are a significant sink of atmospheric CO₂, ergo buffering the anthropogenic increase of this
820 flux. While tropical forests contribute substantially to the global land C sink, observational studies show that a
821 stalled increase in carbon gains over the recent decade (Brienen *et al.*, 2015; Hubau *et al.*, 2020). However
822 modelling studies that lack representation of P cycling processes predict an increasing sink (Fernández-Martínez
823 *et al.*, 2019; Fleischer *et al.*, 2019). This is particularly relevant for efforts to mitigate dangerous climate change
824 and assumptions on the future efficacy of the land C sink. Therefore, in this study, we presented the full
825 terrestrial P cycling and its feedback on the C cycle within the JULES framework. Our results show that the
826 model is capable of representing plant and soil P pools and fluxes at a site in Central Amazon. Moreover, the
827 model estimated a significant NPP limitation under ambient CO₂, due to the high P deficiency at this site which
828 is representative of Central Amazon, and elevated CO₂ resulted in a further subsequent decrease in the land C
829 sink capacity relative to the model without P limitation. While our study is a corner stone for full nutrient
830 cycling representation in ESMs, it can also help the empirical community to test different hypotheses (i.e.,
831 dynamic allocation and stoichiometry) and generate targeted experimental measurements (Medlyn *et al.*, 2015).
832

833 Code and data availability

834 The modified version of JULES vn5_5 and the P extension developed for this paper can be found on Met Office
835 Science Repository Service:
836 https://code.metoffice.gov.uk/svn/jules/main/branches/dev/mahdinakhavali/vn5.5_JULES_PM_NAKHAVALI/
837 (registration is required). Codes for compiling model available at: (<https://doi.org/10.5281/zenodo.5711160>).
838 Simulations were conducted using two sets of model configurations (namelists): ambient CO₂ condition
839 (<https://doi.org/10.5281/zenodo.5711144>) and elevated CO₂ condition
840 (<https://doi.org/10.5281/zenodo.5711150>). The model outputs related to the results in this paper are provided on
841 Zenodo repository (<https://doi.org/10.5281/zenodo.5710898>). All the R scripts used for processing the model
842 outputs and producing results in form of table or figures are provided on Zenodo repository
843 (<https://doi.org/10.5281/zenodo.5710896>).

844 *Author contributions.* MAN, LMM, SS, SEC, CAQ, AJW, IAP, KMA and DBC developed the model, per-
845 formed simulations and analysis. CAQ, FVC, RP, LFL, KMA, GR, LS, ACMM, JSR, RA and JLC provided the
846 measurements for the model parasitisation and evaluation. MAN, LMM, SS, IAP, SEC, FVC, RP, LFL, KMA
847 and DBC contributed in writing the manuscript.
848

849 *Competing interests.* The authors declare no competing interests
850

851 *Acknowledgments.* This work and its contributors (MAN, LMM, KMA and IPH) were supported by the UK
852 Natural Environment Research Council (NERC) grant no NE/LE007223/1. MAN, LMM, SS, IPH were also
853 supported by the Newton Fund through the Met Office Climate Science for Service Partnership Brazil (CSSP
854 Brazil). LMM acknowledges support from the Natural Environment Research Council, grant NEC05816 LTS-
855 M-UKESM. LFL was also supported by AmazonFACE programme (CAPES) and the National Institute of
856 Amazonian Research, grant no: 88887.154643/2017-00. The authors acknowledge contributions from Celso
857 Von Randow towards data curation of the meteorological forcing used in this study and Daniel Goll for
858 modelling insight. We would like to thank Alessandro C. de Araújo and the Large-Scale Biosphere-Atmosphere
859 Program (LBA), coordinated by the National Institute for Amazon Researches (INPA), for the use and
860 availability of data.



861 **References:**

- 862
- 863 Anav, A. *et al.* (2013) ‘Evaluating the land and ocean components of the global carbon cycle in the CMIP5 earth
864 system models’, *Journal of Climate*, 26(18), pp. 6801–6843. doi: 10.1175/JCLI-D-12-00417.1.
- 865 Aragão, L. E. O. C. *et al.* (2009) ‘Above- and below-ground net primary productivity across ten Amazonian
866 forests on contrasting soils’, *Biogeosciences Discussions*, 6(1), pp. 2441–2488. doi: 10.5194/bgd-6-2441-2009.
- 867 Aragão, L. E. O. C. *et al.* (2009) ‘Above- and below-ground net primary productivity across ten Amazonian
868 forests on contrasting soils’, *Biogeosciences*, 6(12), pp. 2759–2778. doi: 10.5194/bg-6-2759-2009.
- 869 Araújo, A. C. *et al.* (2002) ‘Comparative measurements of carbon dioxide fluxes from two nearby towers in a
870 central Amazonian rainforest: The Manaus LBA site’, *Journal of Geophysical Research*, 107(D20), p. 8090.
871 doi: 10.1029/2001JD000676.
- 872 Argles, A. P. K. *et al.* (2020) ‘Robust Ecosystem Demography (RED version 1.0): A parsimonious approach to
873 modelling vegetation dynamics in Earth system models’, *Geoscientific Model Development*, 13(9), pp. 4067–
874 4089. doi: 10.5194/gmd-13-4067-2020.
- 875 Arora, V. K. *et al.* (2020) ‘Carbon–concentration and carbon–climate feedbacks in CMIP6 models and their
876 comparison to CMIP5 models’, *Biogeosciences*, 17(16), pp. 4173–4222. doi: 10.5194/bg-17-4173-2020.
- 877 Baig, S. *et al.* (2015) ‘Does the growth response of woody plants to elevated CO₂ increase with temperature? A
878 model-oriented meta-analysis’, *Global Change Biology*, 21(12), pp. 4303–4319. doi: 10.1111/gcb.12962.
- 879 Baker, T. R. *et al.* (2004) ‘Variation in wood density determines spatial patterns in Amazonian forest biomass’,
880 *Global Change Biology*, 10(5), pp. 545–562. doi: 10.1111/j.1365-2486.2004.00751.x.
- 881 Best, M. J. *et al.* (2011) ‘The Joint UK Land Environment Simulator (JULES), model description – Part 1:
882 Carbon fluxes and vegetation dynamics’, *Geoscientific Model Development*, 4(3), pp. 701–722. doi:
883 10.5194/gmd-4-701-2011.
- 884 Bradford, M. A. and Crowther, T. W. (2013) ‘Carbon use efficiency and storage in terrestrial ecosystems’, *New
885 Phytologist*, 199(1), pp. 7–9. doi: 10.1111/nph.12334.
- 886 Brienen, R. J. W. *et al.* (2015) ‘Long-term decline of the Amazon carbon sink’, *Nature*, 519(7543), pp. 344–
887 348. doi: 10.1038/nature14283.
- 888 Burke, E. J., Chadburn, S. E. and Ekici, A. (2017) ‘A vertical representation of soil carbon in the JULES land
889 surface scheme (vn4.3-permafrost) with a focus on permafrost regions’, *Geoscientific Model Development*,
890 10(2), pp. 959–975. doi: 10.5194/gmd-10-959-2017.
- 891 Castanho, A. D. A. *et al.* (2013) ‘Improving simulated Amazon forest biomass and productivity by including
892 spatial variation in biophysical parameters’, *Biogeosciences*, 10(4), pp. 2255–2272. doi: 10.5194/bg-10-2255-
893 2013.
- 894 Chapin, F. S. *et al.* (2011) *Principles of Terrestrial Ecosystem Ecology*. Springer New York (Biomedical and
895 Life Sciences). Available at: <https://books.google.co.uk/books?id=68nFNpceRmIC>.
- 896 Clark, D. B. *et al.* (2011) ‘The Joint UK Land Environment Simulator (JULES), model description – Part 2:
897 Carbon fluxes and vegetation dynamics’, *Geoscientific Model Development*, 4(3), pp. 701–722. doi:
898 10.5194/gmd-4-701-2011.
- 899 Cleveland, C. C. *et al.* (2015) ‘A comparison of plot-based satellite and Earth system model estimates of tropical
900 forest net primary production’, *Global Biogeochemical Cycles*, 29(5), pp. 626–644. doi:
901 10.1002/2014GB005022.
- 902 Costa, M. G. *et al.* (2016) ‘Labile and Non-Labile Fractions of Phosphorus and Its Transformations in Soil
903 under Eucalyptus’, pp. 1–15. doi: 10.3390/f7010015.
- 904 DeLuca, T. H., Keeney, D. R. and McCarty, G. W. (1992) ‘Effect of freeze-thaw-events on mineralization of
905 soil nitrogen’, *Biol. Fertil. Soils*, 14, pp. 116–120. doi: 10.1007/BF00336260.
- 906 Ellsworth, D. S. *et al.* (2017) ‘Elevated CO₂ does not increase eucalypt forest productivity on a low-phosphorus
907 soil’, *Nature Climate Change*, 7(4), pp. 279–282. doi: 10.1038/nclimate3235.
- 908 Elser, J. J. *et al.* (2007) ‘Global analysis of nitrogen and phosphorus limitation of primary producers in
909 freshwater, marine and terrestrial ecosystems’, *Ecology Letters*, 10(12), pp. 1135–1142. doi: 10.1111/j.1461-
910 0248.2007.01113.x.
- 911 Fernández-Martínez, M. *et al.* (2019) ‘Global trends in carbon sinks and their relationships with CO₂ and
912 temperature’, *Nature Climate Change*, 9(1), pp. 73–79. doi: 10.1038/s41558-018-0367-7.
- 913 Fleischer, K. *et al.* (2019) ‘Amazon forest response to CO₂ fertilization dependent on plant phosphorus
914 acquisition’, *Nature Geoscience*. doi: 10.1038/s41561-019-0404-9.
- 915 Friedlingstein, P. *et al.* (2006) ‘Climate-carbon cycle feedback analysis: Results from the C4MIP model
916 intercomparison’, *Journal of Climate*, 19(14), pp. 3337–3353. doi: 10.1175/JCLI3800.1.
- 917 Friedlingstein, P. *et al.* (2019) ‘Comment on “The global tree restoration potential”’, *Science*. doi:
918 10.1126/science.aay8060.
- 919 Fyllas, N. M. *et al.* (2009) ‘Basin-wide variations in foliar properties of Amazonian forest: phylogeny, soils and
920 climate’, *Biogeosciences*, 6(11), pp. 2677–2708. doi: 10.5194/bg-6-2677-2009.



- 921 Gentile, R. *et al.* (2012) ‘Effects of long-term exposure to enriched CO₂ on the nutrient-supplying capacity of a
922 grassland soil’, *Biology and Fertility of Soils*, 48(3), pp. 357–362. doi: <http://dx.doi.org/10.1007/s00374-011-0616-7>.
923
- 924 Goll, D. S. *et al.* (2017) ‘A representation of the phosphorus cycle for ORCHIDEE (revision 4520)’,
925 *Geoscientific Model Development*, 10(10), pp. 3745–3770. doi: 10.5194/gmd-10-3745-2017.
- 926 Harper, A. B. *et al.* (2016) ‘Improved representation of plant functional types and physiology in the Joint UK
927 Land Environment Simulator (JULES v4.2) using plant trait information’, *Geoscientific Model Development*,
928 9(7), pp. 2415–2440. doi: 10.5194/gmd-9-2415-2016.
- 929 Hatfield, J. L. and Dold, C. (2019) ‘Water-use efficiency: Advances and challenges in a changing climate’,
930 *Frontiers in Plant Science*, 10(February), pp. 1–14. doi: 10.3389/fpls.2019.00103.
- 931 Haverd, V. *et al.* (2018) ‘A new version of the CABLE land surface model (Subversion revision r4601)
932 incorporating land use and land cover change, woody vegetation demography, and a novel optimisation-based
933 approach to plant coordination of photosynthesis’, *Geoscientific Model Development*, 11(7), pp. 2995–3026.
934 doi: 10.5194/gmd-11-2995-2018.
- 935 He, M. and Dijkstra, F. A. (2014) ‘Drought effect on plant nitrogen and phosphorus: A meta-analysis’, *New
936 Phytologist*, 204(4), pp. 924–931. doi: 10.1111/nph.12952.
- 937 Hedley, M. J., Stewart, J. W. B. and Chauhan, B. S. (1982) ‘Changes in Inorganic and Organic Soil Phosphorus
938 Fractions Induced by Cultivation Practices and by Laboratory Incubations’, *Soil Science Society of America
939 Journal*, 46(5), pp. 970–976. doi: <https://doi.org/10.2136/sssaj1982.03615995004600050017x>.
- 940 Hou, E. *et al.* (2019) ‘Quantifying Soil Phosphorus Dynamics: A Data Assimilation Approach’, *Journal of
941 Geophysical Research: Biogeosciences*, pp. 1–15. doi: 10.1029/2018jg004903.
- 942 Hubau, W. *et al.* (2020) ‘Asynchronous carbon sink saturation in African and Amazonian tropical forests’,
943 *Nature*, 579(7797), pp. 80–87. doi: 10.1038/s41586-020-2035-0.
- 944 Hungate, B. a *et al.* (2003) ‘Nitrogen and Climate Change’, *Science*, 302(November), pp. 1512–1513.
- 945 Jenkinson, D. S. *et al.* (1990) ‘The turnover of organic carbon and nitrogen in soil’, *The Royal Society*,
946 329(1255). doi: <https://doi.org/10.1098/rstb.1990.0177>.
- 947 Jenkinson, D. S. and Coleman, K. (2008) ‘The turnover of organic carbon in subsoils. Part 2. Modelling carbon
948 turnover’, *European Journal of Soil Science*, 59(2), pp. 400–413. doi: 10.1111/j.1365-2389.2008.01026.x.
- 949 Jiang, M. *et al.* (2019) ‘Towards a more physiological representation of vegetation phosphorus processes in land
950 surface models’, *New Phytologist*, 222(3), pp. 1223–1229. doi: 10.1111/nph.15688.
- 951 Jiang, M. *et al.* (2020) ‘The fate of carbon in a mature forest under carbon dioxide enrichment’, *Nature*,
952 580(7802), pp. 227–231. doi: 10.1038/s41586-020-2128-9.
- 953 Johnson, M. O. *et al.* (2016) ‘Variation in stem mortality rates determines patterns of above-ground biomass in
954 Amazonian forests: implications for dynamic global vegetation models’, *Global Change Biology*, 22(12), pp.
955 3996–4013. doi: 10.1111/gcb.13315.
- 956 Kattge, J. *et al.* (2009) ‘Quantifying photosynthetic capacity and its relationship to leaf nitrogen content for
957 global-scale terrestrial biosphere models’, *Global Change Biology*, 15(4), pp. 976–991. doi:
958 <https://doi.org/10.1111/j.1365-2486.2008.01744.x>.
- 959 Keller, M. *et al.* (2004) ‘Ecological research in the Large-scale Biosphere-Atmosphere Experiment in
960 Amazonia: Early results’, *Ecological Applications*, 14(4 SUPPL.), pp. 3–16. doi: 10.1890/03-6003.
- 961 Klein, T. *et al.* (2016) ‘Growth and carbon relations of mature *Picea abies* trees under 5 years of free-air CO₂
962 enrichment’, *Journal of Ecology*, 104(6), pp. 1720–1733. doi: 10.1111/1365-2745.12621.
- 963 Koch, A., Hubau, W. and Lewis, S. L. (2021) ‘Earth System Models Are Not Capturing Present-Day Tropical
964 Forest Carbon Dynamics’, *Earth’s Future*, 9(5), pp. 1–19. doi: 10.1029/2020EF001874.
- 965 Körner, C. *et al.* (2005) ‘Ecology: Carbon flux and growth in mature deciduous forest trees exposed to elevated
966 CO₂’, *Science*, 309(5739), pp. 1360–1362. doi: 10.1126/science.1113977.
- 967 Lapola, D. M. and Norby, R. (2014) ‘Assessing the effects of increased atmospheric CO₂ on the ecology and
968 resilience of the Amazon forest’, *Science plan et implementation strategy*, AMAZON FAC.
- 969 LeBauer, D. and Treseder, K. (2008) ‘Nitrogen Limitation of Net Primary Productivity’, *Ecology*, 89(2), pp.
970 371–379.
- 971 Lloyd, J. *et al.* (2001) ‘Should Phosphorus Availability Be Constraining Moist Tropical Forest Responses to
972 Increasing CO₂ Concentrations?’, in *Global Biogeochemical Cycles in the Climate System*. Elsevier, pp. 95–
973 114. doi: 10.1016/B978-012631260-7/50010-8.
- 974 De Lucia, E. H. *et al.* (2007) ‘Forest carbon use efficiency: Is respiration a constant fraction of gross primary
975 production?’, *Global Change Biology*, 13(6), pp. 1157–1167. doi: 10.1111/j.1365-2486.2007.01365.x.
- 976 Lugli, L. F. (2013) *Estoque de nutrientes na serrapilheira fina e grossa em função de fatores edáficos em
977 florestas do Amazonas, Brasil*. Instituto Nacional de Pesquisas da Amazônia - INPA. Available at:
978 <https://repositorio.inpa.gov.br/handle/1/5028>.
- 979 Lugli, L. F. *et al.* (2021) ‘Rapid responses of root traits and productivity to phosphorus and cation additions in a
980 tropical lowland forest in Amazonia’, *New Phytologist*, 230(1), pp. 116–128. doi: 10.1111/nph.17154.



- 981 Luo, Y. *et al.* (2004) ‘Progressive nitrogen limitation of ecosystem responses to rising atmospheric carbon
982 dioxide’, *BioScience*, 54(8), pp. 731–739. doi: 10.1641/0006-3568(2004)054[0731:PNLOER]2.0.CO;2.
- 983 Malhi, Y. *et al.* (2004) ‘The above-ground coarse wood productivity of 104 Neotropical forest plots’, *Global*
984 *Change Biology*, 10(5), pp. 563–591. doi: 10.1111/j.1529-8817.2003.00778.x.
- 985 Malhi, Y. *et al.* (2006) ‘The regional variation of aboveground live biomass in old-growth Amazonian forests’,
986 *Global Change Biology*, 12(7), pp. 1107–1138. doi: 10.1111/j.1365-2486.2006.01120.x.
- 987 Malhi, Y. *et al.* (2009) ‘Comprehensive assessment of carbon productivity, allocation and storage in three
988 Amazonian forests’, *Global Change Biology*, 15(5), pp. 1255–1274. doi: 10.1111/j.1365-2486.2008.01780.x.
- 989 Malhi, Y. (2012) ‘The productivity, metabolism and carbon cycle of tropical forest vegetation’, *Journal of*
990 *Ecology*, 100(1), pp. 65–75. doi: 10.1111/j.1365-2745.2011.01916.x.
- 991 Malhi, Y., Doughty, C. and Galbraith, D. (2011) ‘The allocation of ecosystem net primary productivity in
992 tropical forests’, *Philosophical Transactions of the Royal Society B: Biological Sciences*, 366(1582), pp. 3225–
993 3245. doi: 10.1098/rstb.2011.0062.
- 994 Medlyn, B. E. *et al.* (2015) ‘Using ecosystem experiments to improve vegetation models’, *Nature Climate*
995 *Change*, 5(6), pp. 528–534. doi: 10.1038/nclimate2621.
- 996 Medlyn, B. E. *et al.* (2016) ‘Using models to guide field experiments: a priori predictions for the CO₂ response
997 of a nutrient- and water-limited native Eucalypt woodland’, *Global Change Biology*, 22(8), pp. 2834–2851. doi:
998 10.1111/gcb.13268.
- 999 Mercado, L. M. *et al.* (2011) ‘Variations in Amazon forest productivity correlated with foliar nutrients and
1000 modelled rates of photosynthetic carbon supply’, *Philosophical Transactions of the Royal Society B: Biological*
1001 *Sciences*, 366(1582), pp. 3316–3329. doi: 10.1098/rstb.2011.0045.
- 1002 Mitchard, E. T. A. (2018) ‘The tropical forest carbon cycle and climate change’, *Nature*, 559(7715), pp. 527–
1003 534. doi: 10.1038/s41586-018-0300-2.
- 1004 Norby, R. J. *et al.* (2016) ‘Model–data synthesis for the next generation of forest free-air ^{CO}₂
1005 enrichment (^{FACE}) experiments’, *New Phytologist*, 209(1), pp. 17–28. doi: 10.1111/nph.13593.
- 1006 Nordin, A., Höglberg, P. and Näsholm, T. (2001) ‘Soil nitrogen form and plant nitrogen uptake along a boreal
1007 forest productivity gradient’, *Oecologia*, 129(1), pp. 125–132. doi: 10.1007/s004420100698.
- 1008 Pan, Y. *et al.* (2011) ‘A Large and Persistent Carbon Sink in the World’s Forests’, *Science*, 333(6045), pp. 988–
1009 993. doi: 10.1126/science.1201609.
- 1010 Perakis, S. S. and Hedin, L. O. (2002) ‘Nitrogen loss from unpolluted South American forests mainly via
1011 dissolved organic compounds’, *Nature*, 415(6870), pp. 416–419. doi: 10.1038/415416a.
- 1012 Phillips, O. L. *et al.* (2004) ‘Pattern and process in Amazon tree turnover, 1976–2001’, *Philosophical*
1013 *Transactions of the Royal Society B: Biological Sciences*, 359(1443), pp. 381–407. doi: 10.1098/rstb.2003.1438.
- 1014 Phillips, O. L. *et al.* (2017) ‘Carbon uptake by mature Amazon forests has mitigated Amazon nations’ carbon
1015 emissions’, *Carbon Balance and Management*, 12(1), pp. 1–9. doi: 10.1186/s13021-016-0069-2.
- 1016 Quesada, C. A. *et al.* (2010) ‘Variations in chemical and physical properties of Amazon forest soils in relation to
1017 their genesis’, *Biogeosciences*, 7(5), pp. 1515–1541. doi: 10.5194/bg-7-1515-2010.
- 1018 Quesada, C. A. *et al.* (2011) ‘Soils of Amazonia with particular reference to the RAINFOR sites’,
1019 *Biogeosciences*, 8(6), pp. 1415–1440. doi: 10.5194/bg-8-1415-2011.
- 1020 Quesada, C. A. *et al.* (2012) ‘Basin-wide variations in Amazon forest structure and function are mediated by
1021 both soils and climate’, *Biogeosciences*, 9(6), pp. 2203–2246. doi: 10.5194/bg-9-2203-2012.
- 1022 Reed, S. C., Yang, X. and Thornton, P. E. (2015) ‘Incorporating phosphorus cycling into global modeling
1023 efforts: A worthwhile, tractable endeavor’, *New Phytologist*, 208(2), pp. 324–329. doi: 10.1111/nph.13521.
- 1024 Ryan, M. G. (2013) ‘Three decades of research at Flakaliden advancing whole-tree physiology, forest ecosystem
1025 and global change research’, *Tree Physiology*, 33(11), pp. 1123–1131. doi: 10.1093/treephys/tpt100.
- 1026 Sampaio, G. *et al.* (2021) ‘CO₂ physiological effect can cause rainfall decrease as strong as large-scale
1027 deforestation in the Amazon’, *Biogeosciences*, 18(8), pp. 2511–2525. doi: 10.5194/bg-18-2511-2021.
- 1028 Sanchez, P. A. (1977) ‘Properties and Management of Soils in the Tropics’, *Soil Science*, 124(3). Available at:
1029 https://journals.lww.com/soilsci/Fulltext/1977/09000/Properties_and_Management_of_Soils_in_the_Tropics.12.aspx.
- 1030
- 1031 Sardans, J., Rivas-Ubach, A. and Peñuelas, J. (2012) ‘The C:N:P stoichiometry of organisms and ecosystems in
1032 a changing world: A review and perspectives’, *Perspectives in Plant Ecology, Evolution and Systematics*, 14(1),
1033 pp. 33–47. doi: 10.1016/j.ppees.2011.08.002.
- 1034 Schimel, D., Stephens, B. B. and Fisher, J. B. (2015) ‘Effect of increasing CO₂ on the terrestrial carbon cycle’,
1035 *Proceedings of the National Academy of Sciences of the United States of America*, 112(2), pp. 436–441. doi:
1036 10.1073/pnas.1407302112.
- 1037 Shen, J. *et al.* (2011) ‘Phosphorus dynamics: From soil to plant’, *Plant Physiology*, 156(3), pp. 997–1005. doi:
1038 10.1104/pp.111.175232.
- 1039 Sitch, S. *et al.* (2008) ‘Evaluation of the terrestrial carbon cycle, future plant geography and climate-carbon
1040 cycle feedbacks using five Dynamic Global Vegetation Models (DGVMs)’, *Global Change Biology*, 14(9), pp.



- 1041 2015–2039. doi: 10.1111/j.1365-2486.2008.01626.x.
1042 Stephenson, N. L. and Van Mantgem, P. J. (2005) ‘Forest turnover rates follow global and regional patterns of
1043 productivity’, *Ecology Letters*, 8(5), pp. 524–531. doi: 10.1111/j.1461-0248.2005.00746.x.
1044 Tian, J. *et al.* (2017) ‘Accumulation and distribution of phosphorus in the soil profile under fertilized grazed
1045 pasture’, *Agriculture, Ecosystems and Environment*, 239, pp. 228–235. doi: 10.1016/j.agee.2017.01.022.
1046 Vitousek, P. M. *et al.* (1997) ‘Human Domination of Earth Ecosystems’, *Science*, 278(5335), p. 21. Available
1047 at: <http://www.cheric.org/research/tech/periodicals/view.php?seq=257860>.
1048 Vitousek, P. M. *et al.* (2010) ‘Terrestrial phosphorus limitation: Mechanisms, implications, and nitrogen-
1049 phosphorus interactions’, *Ecological Applications*, 20(1), pp. 5–15. doi: 10.1890/08-0127.1.
1050 Vitousek, P. M. and Howarth, R. W. (1991) ‘Nitrogen limitation on land and in the sea: How can it occur?’,
1051 *Biogeochemistry*, 13(2), pp. 87–115. doi: 10.1007/BF00002772.
1052 Walker, A. P. *et al.* (2021) ‘Integrating the evidence for a terrestrial carbon sink caused by increasing
1053 atmospheric CO₂’, *New Phytologist*, 229(5), pp. 2413–2445. doi: 10.1111/nph.16866.
1054 Walker, T. W. and Syers, J. K. (1976) ‘The fate of phosphorus during pedogenesis’, *Geoderma*, 15(1), pp. 1–19.
1055 doi: 10.1016/0016-7061(76)90066-5.
1056 Wang, Y.-P. and Goll, D. S. (2021) ‘Modelling of land nutrient cycles: recent progress and future development’,
1057 *Faculty Reviews*, 10(53). doi: 10.12703/r/10-53.
1058 Wang, Y. P., Law, R. M. and Pak, B. (2010) ‘A global model of carbon, nitrogen and phosphorus cycles for the
1059 terrestrial biosphere’, *Biogeosciences*, 7(7), pp. 2261–2282. doi: 10.5194/bg-7-2261-2010.
1060 Wiltshire, A. J. *et al.* (2021) ‘Jules-cn: A coupled terrestrial carbon-nitrogen scheme (jules vn5.1)’,
1061 *Geoscientific Model Development*, 14(4), pp. 2161–2186. doi: 10.5194/gmd-14-2161-2021.
1062 Xiao, J. *et al.* (2013) ‘Carbon fluxes, evapotranspiration, and water use efficiency of terrestrial ecosystems in
1063 China’, *Agricultural and Forest Meteorology*, 182–183, pp. 76–90. doi: 10.1016/j.agrformet.2013.08.007.
1064 Xu, Z. *et al.* (2016) ‘Elevated-CO₂ response of stomata and its dependence on environmental factors’, *Frontiers*
1065 *in Plant Science*, 7(MAY2016), pp. 1–15. doi: 10.3389/fpls.2016.00657.
1066 Yang, X. *et al.* (2013) ‘The distribution of soil phosphorus for global biogeochemical modeling’,
1067 *Biogeosciences*, 10(4), pp. 2525–2537. doi: 10.5194/bg-10-2525-2013.
1068 Yang, X. *et al.* (2014) ‘The role of phosphorus dynamics in tropical forests – a modeling study using CLM-
1069 CNP’, *Biogeosciences*, 11(6), pp. 1667–1681. doi: 10.5194/bg-11-1667-2014.
1070 Yang, X. and Post, W. M. (2011) ‘Phosphorus transformations as a function of pedogenesis: A synthesis of soil
1071 phosphorus data using Hedley fractionation method’, *Biogeosciences*, 8(10), pp. 2907–2916. doi: 10.5194/bg-8-
1072 2907-2011.
1073 Zaehle, S. and Dalmonech, D. (2011) ‘Carbon-nitrogen interactions on land at global scales: Current
1074 understanding in modelling climate biosphere feedbacks’, *Current Opinion in Environmental Sustainability*,
1075 3(5), pp. 311–320. doi: 10.1016/j.cosust.2011.08.008.
1076 Zaehle, S. and Friend, A. D. (2010) ‘Carbon and nitrogen cycle dynamics in the O-CN land surface model: 1.
1077 Model description, site-scale evaluation, and sensitivity to parameter estimates’, *Global Biogeochemical Cycles*,
1078 24(1), pp. 1–13. doi: 10.1029/2009GB003521.
1079 Zhu, Q. *et al.* (2016) ‘Multiple soil nutrient competition between plants, microbes, and mineral surfaces: model
1080 development, parameterization, and example applications in several tropical forests’, *Biogeosciences*, 13(1), pp.
1081 341–363. doi: 10.5194/bg-13-341-2016.
1082